Case Studies in Construction Materials 17 (2022) e01202

Contents lists available at ScienceDirect

Case Studies in Construction Materials

journal homepage: www.elsevier.com/locate/cscm

Structural validation of geothermal water basins constructed with durability enhanced ultra high performance fiber reinforced concrete (Ultra High Durability Concrete)

Salam Al-Obaidi [a,b,*], Marco Davolio [a], Francesco Lo Monte [a], Ferdinando Costanzi [c], Massimo Luchini [c], Patrick Bamonte [a], Liberato Ferrara [a]

[a] Department of Civil and Environmental Engineering, Politecnico di Milano, Piazza Leonardo DaVinci 32, Milan 20133, Italy
[b] Roads and Transportations Engineering Department, University of Al-Qadisiyah, Diwaniyah 58001, Iraq
[c] Enel Green Power (EGP)-Innovation and Sustainability (I&S), Rome 00198, Italy

ARTICLE INFO

Keywords:
Durability
UHPFRC
Water-retaining structures
Performance based design

ABSTRACT

Ultra-High Performance Concrete (UHPC) proved to be very durable in harsh environments, primarily because of the extremely low porosity of the matrix (uncracked). However, the limited availability of design standards is still a barrier to widespread applications of UHPC, together with still limited knowledge of its durability in the real (cracked) service conditions. In this paper, the use of tailored UHPC is introduced, whose composition has been specifically designed to achieve enhanced durability in the cracked state combined with extremely aggressive environments. Validation of the material and structural design concept on a full scale structure is presented, with reference to a tank intended to contain geothermal water from the cooling tower at a geothermal power plant. This pilot structure was designed and constructed using both ordinary reinforced concrete and durability enhanced UHPC, which is called hereafter Ultra High Durability Concrete (UHDC), for comparative assessment purposes. Upon the completion of the pilot construction and entering its service life, periodic assessment and validation tests have been carried out to validate the structural design assumptions and to check the serviceability requirements. Results of these tests, performed over the span of two years are reported in detail in this paper to validate the material and structural concepts. The study highlights the most important parameters that could affect the performance of UHPC structures during casting and service life. The overall project framework presented in this paper has to be intended as a pioneer study in moving towards a performance based durability-design approach for UHPC structures.

1. Introduction

The durability performance of concrete is attracting more intense research attention and efforts over the years. The final main aim of these efforts is to provide structural engineers with tools enabling them to predict the evolution of the structural performance over time, as affected by the defined degradation mechanisms, and quantify the structural service life. This is defined as the time when the

* Corresponding author at: Department of Civil and Environmental Engineering, Politecnico di Milano, Piazza Leonardo DaVinci 32, Milan 20133, Italy.
E-mail address: salammaytham.alobaidi@polimi.it (S. Al-Obaidi).

https://doi.org/10.1016/j.cscm.2022.e01202
Received 30 March 2022; Received in revised form 24 May 2022; Accepted 26 May 2022
Available online 31 May 2022

structural performance does no longer fulfill the demanded requirements, with the intended safety margin [1]. Since deterioration of the concrete materials can severely impair the structural performance at serviceability limit state, the same tools can be also effectively employed as decision making tools to plan the maintenance and the retrofitting process to restore at least the original structural functionality [2]. In current design codes, the durability design is often tackled through deemed to satisfy prescriptions [3], that implicitly aim at achieving the target service life. The aforesaid prescriptions have inherent uncertainty, being based on individual research circumstances while aiming to cover a broad variety of structural applications, merely classified through widely defined environmental exposure classes [4]. This may result into the same prescriptions failing to guarantee the target service life, which may require expensive corrective and/or preventive maintenance operations. For example, in chemical plants, these can reach, according to Nguyen et al. [5], 30% of the annual operational budget. Repair and reconstruction of these infrastructures with the same materials and design concept as the original one will not solve the issue, but will exaggerate the problem of economic and resources consumption.

As a matter of fact, the main driver of degradation mechanisms in concrete is the transport of aggressive agents, including, e.g., chloride and sulfate ions, through the porous structure of the concrete (cement paste) matrix as well as through the cracks whose formation and presence characterizes the service state of a concrete structure [6,7]. The use of Ultra High Performance Concrete (UHPC) [8] can provide twofold benefit in this respect due to both its inherent low porosity, thanks to particle-packing based mix-design concepts employed to design its composition, and to the use of micro-fibers. The fibers, generally made of steel though applications with polymer fibers are increasing, are providing the tensile strain hardening behavior, spreading an otherwise localized damage into multiple tiny opened and tightly spaced cracks, much tinier and tighter than what obtainable in ordinary reinforced concrete structures even with the most carefully designed and detailed reinforcement [9–11]. Nonetheless, despite the aforesaid features that make UHPC highly attractive for structural applications in aggressive environments [12], its wide use is still in the low range, especially in Europe, where it has been extensively applied mainly in bridge deck retrofitting and upgrading as well as in other kinds of structural repair applications [7,8]. This has been mainly due to high cost of its ingredients together with limited awareness and, until very recent times, to the lack of internationally recognized codes for the structural design and approval [13]. As a matter of fact, while such a lag in widespread and full structural applications of advanced (cement-based) construction materials and technologies can be recognized as a common denominator in several innovations in structural engineering (name, for example, the diffusion and acceptance of pre-stressed concrete and fiber reinforced concrete in the first and second half of XX century respectively), in the authors' opinion, and in the case of UHPC this is also due to two misperceptions. On the one hand, the cost assessment is often made on the basis of the material cost per unit volume (€ or $/m3) and simply referred to construction costs, whereas the superior mechanical (and durability) performance of UHPC could allow, as it does, to build with lower material quantities while guaranteeing the same structural performance and longer service life. This would require a cost-assessment to be based on a functional unit (e.g. the structure, as designed and built) and on a life-cycle basis [2,14,15]. On the other hand, in order to bring UHPC to an as broad as possible market, its use has not to be foreseen just for mere incremental upgrading of existing structural concepts, and then confined to reduction of reinforcement cover and element thicknesses, but as a driver to realize innovative structure concepts. This also in synergy with tailored construction technologies including prefabrication and additive manufacturing, whose implementation would not be otherwise feasible [16–20].

All what above said converges towards the need to deepen the knowledge, and work out the development of related predictive design models, of the UHPC material and structural behavior not only with reference to the ultimate limit states, but also, if not primarily, in the service scenarios. These have to include on the one hand the interaction of the material in its cracked state with the environmental conditions, and environment-born aggressors. Moreover, careful considerations are required on how the employed construction technologies and processes do affect the reliability with the load resistance mechanisms hypothesized in the design stage. This consideration will be underlined and checked during construction and service stages to actually establish themselves in the structure as built.

In this paper the conceptual framework addressed above will be applied to a real-size case study, whose structure is a pilot tank structure to collect water from cooling towers in a geothermal power plant in Tuscany, Italy, owned and operated by Enel Green Power. The basin is used to contain the geothermal water that comes out of the ground during the drilling process, to store and cool it down before injecting back to the ground. The geothermal water however, contains significant amount of chloride and sulphate ions as reported in Table 1.

The structure has been built as a demonstrator in the framework of the project ReSHEALience ("Rethinking coastal defense and Green-energy Service infrastructures through enHancEd-durAbiLity high-performance cement-based materials), funded by the European Union Horizon 2020 research and innovation program under GA No 760824. The tank, which measures 7.0 m × 22.5 m in plan and is 1.5 m high, is separated into three different compartments, each 7.0 m wide and 7.5 m long. The tank was built by employing different materials and construction technologies, namely:100 mm thick cast-in-place ordinary reinforced concrete walls, 60 mm cast-in-place UHDC walls, and 30 mm thick UHDC precast slabs stiffened by 200 × 200 mm^2 UHDC cast in place columns/buttresses (Fig. 1).

Table 1
Typical compositions of water int geothermal Chiusdino plant owned and operated by EGP.

Compositions	pH	Cl^- mg/L	$S_2O_3^{2-}$ mg/L	SO_3^{2-}mg/L	SO_4^{2-} mg/L	H_2S mg/L	Conductivity μS/cm
Quantity	6.9	1.0	46	325	5.119	1.5	7.87

The assessment of the structure is currently involving multiscale level testing:

- from micro-scale, where the crack width, porosity, permeability, and steel-matrix bond behavior will be examined,
- to meso-scale level, where specimens, of appropriate sizes and casted at the same time and circumstances of the structure have been tested in the laboratory to assess the mechanical and durability material performance and the reliability of structural resistant mechanisms,
- and to macro-scale level, where periodic assessments of the pilot structure have been carried out by filling the tank compartments and measuring the quantities of interest also to assess the evolution of the structural response as affected by the prolonged exposure to aggressive (geothermal) water (between two successive tests the basins were kept full of water).

This paper is going to report a summary of these last macro-scale level tests, also with the aim of verifying the reliability of the material properties, identification procedure, and of the assumptions made in the design stage, mainly with reference to the tailored UHDC materials and structural concepts herein employed.

2. Materials and design

The conceptual framework of the durability-based design approach, described in [21] and employed for the case study at issue, is illustrated in Fig. 2**.** Since the pilot structure was built to demonstrate the use of the UHPC/UHDC materials in full structural applications, all the durability design parameters will be reviewed in this study as they affect the service life of the structure. In previous works [1,21,23,24], conceptual design, preliminary and detailed design have been thoroughly discussed and reported. Therefore, this study is focusing more on construction and service phases.

Since the main goal of the project was to upgrade the durability performance of UHPC, tailored nanoscale constituents either alumina nanofibers (ANF - 0.25% by weight of cement) or cellulose nanocrystals (CNC - 0.15% by weight of cement) were incorporated in the three different mix designs to produce the UHDCs listed in Table 2. All the mixes also contained a crystalline admixture as stimulator of the autogenous healing capacity.

Mechanical properties have been evaluated for these materials at different scale and configurations as shown in Fig. 3, which shows an appreciable ductility performance particularly in the tensile behavior. The durability parameters have also been evaluated and reported in several publications and are summarized in Table 3 [23–32].

The employed UHDC mixes were produced on site, in a geothermal power plant owned by Enel Green Power in Chiusdino, using a dedicated mixing equipment type MAV 1.0 with a maximum capacity of 1.0 m^3 and a power of 50 HP. Batches of half cubic meter each were mixed to ensure the quality of concrete and facilitate the casting process. Giving the proportions of the UHDC ingredients listed in Table 2, a previously calibrated and tailored mixing protocol was implemented to ensure the quality of the intended mixture conditions (Table 4).

The construction phase started first with compacting the soil and casting a lean concrete layer under the 300 mm thick foundation slab, which was built using a C35 concrete. Steel dowels were left protruding from the foundation to be overlapped with the reinforcement of the walls of the first compartment. When casting the foundation, pre-made grooves were prepared to work as an encasing systems for the walls of the second and the third compartments.

The 100 mm thick walls of the first compartment of the basin have been reinforced with two layers of 10 mm steel rebars, with a 30 mm concrete cover. The Eurocode 2 [4] specifies the minimum concrete cover according to the structural classes reported in Table 5: for the case at issue class S4 for a specified service life equal to 50 years was selected at first instance. However, the structural class can be further modified based on specific conditions, as in Table 6. Based on the modified structural class and exposure condition, the wall of the first compartment was assigned to structural class 2 (S2) after applying some of the criteria provided in Table 6, including: member with slab geometry, and special quality control. In fact, the ordinary concrete employed for the construction of the

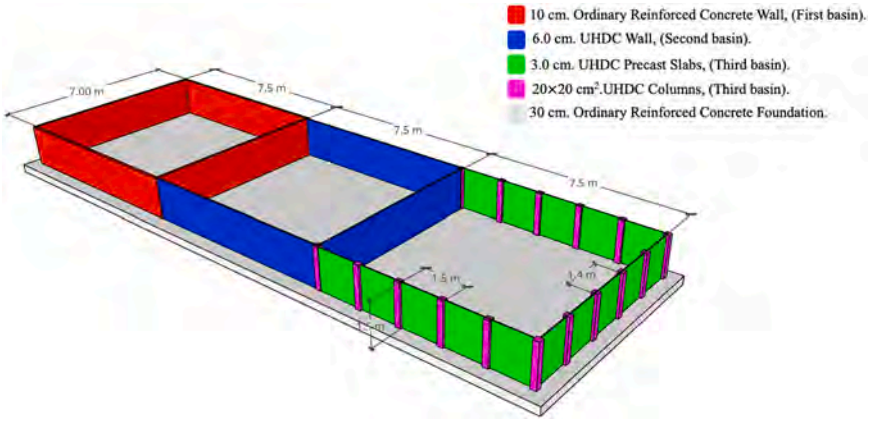

Fig. 1. Schematic of the basin pilot structure with corresponding materials and dimensions.

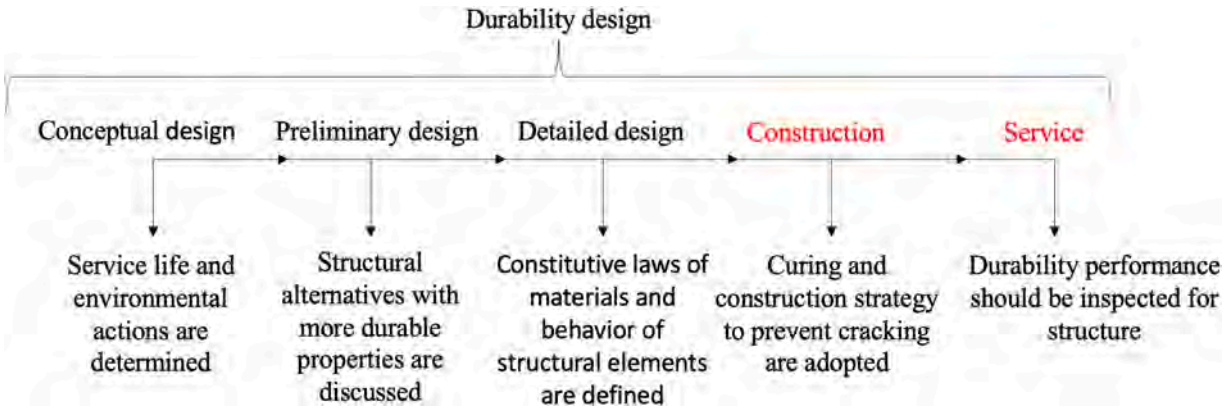

Fig. 2. Durability design framework of concrete structures [21].

Table 2
Employed Ultra-High-Durability Concrete (UHDC) mix compositions (quantities are given in kg/m^3 if not otherwise specified).

Constituents	XA-CA	XA-CA + ANF	XA-CA+CNC
CEM I 52,5R	600	600	600
Slag	500	500	500
Water (litres/m^3)	200	200	200
Steel fibers Azichem Readymesh 200® (l_f/d_f = 20/0.22)	120	120	120
Sand 0–2 mm	982	982	982
Superplasticizer Glenium ACE 300 ® (litres/m^3)	33	33	33
Crystalline Admixture Penetron Admix ®	4.8	4.8	4.8
Alumina nanofibers NAFEN® *	–	0.25	–
Cellulose nano Crystals Navitas® *	–	–	0.15

*% by weight of cement.

wall of the first compartment contained the same crystalline self-healing stimulator employed in the UHDC mixes (Penetron Admix®), at 1% dosage by weight of cement. This was to validate the efficiency of self-healing in allowing a reduction of the concrete cover thickness. Thus, considering an exposure class XD2, a minimum concrete cover of 30 mm was selected. The reinforcement bars of the first compartment were equipped with strain gauges to monitor the corresponding parameters during the service phase.

The 60 mm thick walls of the second compartment were cast in place; the employed UHDC was mixed onsite in 0.5 m^3 batches, as said above, and transported by means of bucket that opens and released the concrete with the aid of a chute inside the wooden molds, Fig. 4a.

The walls of the third compartment consisted of 30 mm thick precast UHDC slabs combined with 200 × 200 mm^2 cast in place UHDC columns to join together the adjacent slabs and provide flexural stiffness for the global composite wall at the same time. The 1,65 × 1,50 m slabs (width x length) were pre-cast (horizontally) on the site, Fig. 4b. After hardening, they were placed vertically in their positions. It is worth remarking that 40 mm diameter holes were "left" on the edges of the slabs to work, once filled by the UHDC mix of columns and of the foundation encasing "kerb", as interlocking dowels: as a matter of fact, the employed UHDC mix, thanks to its self-levelling consistency, can easily fill these holes and integrate the precast elements with the columns, or the foundation encasing system during the casting. Therefore, every pair of adjacent slabs was tightened together by steel straps, then the column wooden molds were erected around the joint to cast the columns (Figs. 4c and 5). Concrete strain gauges were installed on the surface of the second and the third compartment to measure the relative strains during filling of each compartment to validate the design assumptions, as it will be detailed later.

After completion of the tank construction, the works for the installation of feeding, spillage and drainage systems started. The feeding pipes were installed externally and are supplied by a unique external pipe coming from the source, provided with individual valves: in this way they can be opened to fill each compartment independently. Spillage pipes were installed at 1.4 m height from the bottom to take out the water when exceeded the service water level through a drainage hole, where they connected to the main drainage system installed at the base of each basin during the construction of the foundation. The drainage pipes were also provided with external valves, so that they can be easily controlled during filling of the compartment (Fig. 5).

3. Validation tests of the pilot

Upon the completion of the structure and entering its service stage, several tests have been conducted to validate the design assumptions and evaluate the structural response under its service scenario.

Construction of the tank was completed by the end of February 2020; then due to CoViD-19 contingency, installment of fixtures was

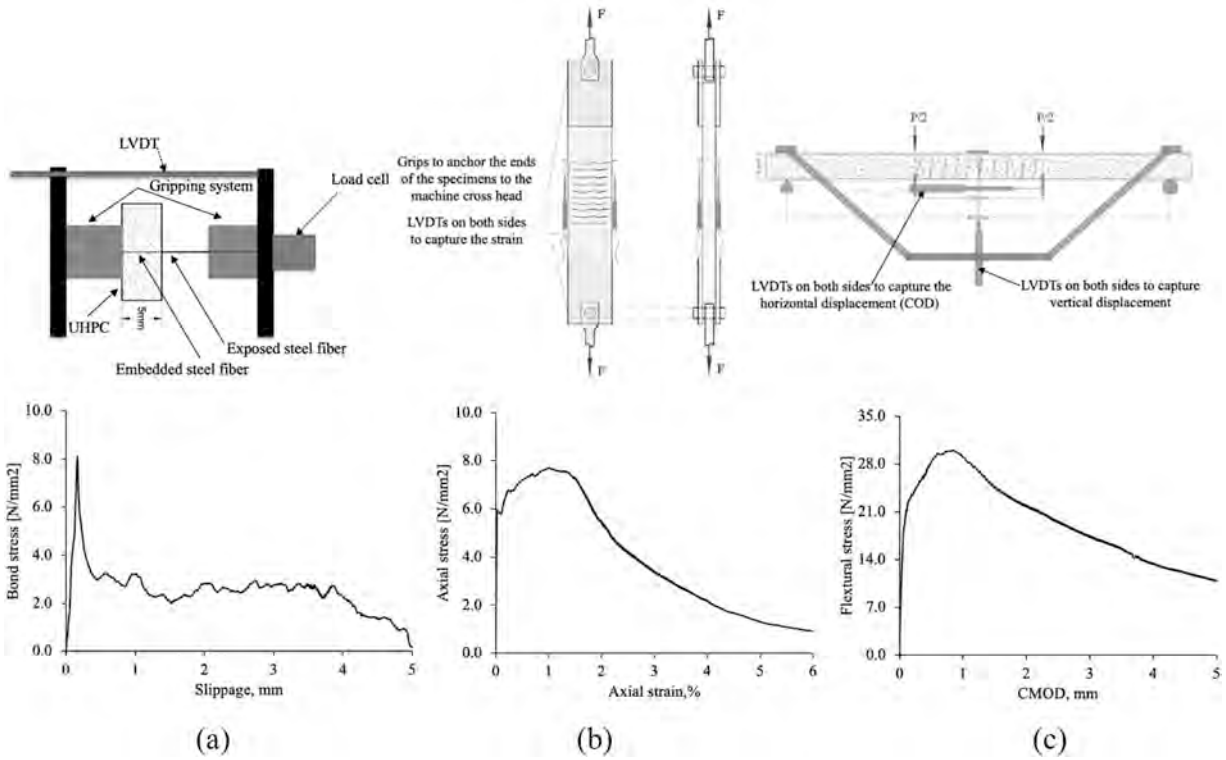

Fig. 3. Mechanical behavior of UHDC samples; (a) single fiber bond-slip curve, (b) tensile-strain curve, and (c) flexural stress-COD curve.

Table 3
The main mechanical and durability parameters of the UHPC [33].

Parameter	Time	XA-CA	XA-CA + ANF	XA-CA+CNC
Total porosity (%)	2 months	4.35	2.98	2.84
	24 months	2.46	2.80	2.86
Compressive strength (MPa)	28 days	126.9	144.9	147.6
	56 days	142.9	155	157
	84 days	166.3	166.5	170.5
Compressive strength(MPa)*	28 days	140.4	123.8	137.3
	56 days	152.8	135.5	147
	84 days	161.4	174.2	169.2
Flexural strength (MPa)	28 days	24.4	23.5	27.3
	56 days	28.9	22.7	21.4
	84 days	29.0	27.9	30.4
Flexural strength (MPa)*	28 days	26.1	29.4	33.7
	56 days	26.2	30.4	34.9
	84 days	27.5	29.8	32.1
Dynamic elastic modulus (MPa)	2 months	52.3	47.8	49.8
	6 months	53.71	49.9	53.26
Electrical resistivity (Ω m)	2 months	31	25	34.3
	6 months	64.8	139	101
Chloride migration coefficient (m^2/s)	2 months	10×10^{-13}	9.2×10^{-13}	13×10^{-13}
Water capillary suction ($kg/m^2\ mln^{0.5}$)	2 months	50×10^{-13}	43×10^{-13}	44×10^{-13}
Crack sealing (%)*	1 month	21.44	36.78	46.74
	3 months	42.08	72.08	91.58
	6 months	51.17	87.66	100
Healing efficiency (%)*	1 month	29.9	35.6	45.0
	3 months	55.5	69.9	84.5
	6 months	63.1	87.1	97.1

* Developed in geothermal water.

Table 4
Mixing and pouring protocol.

Time (min)	Operation
0–2	Dry mixing of cement, slag, CA, and sand
2–3	Add water, Superplasticizer
3–4	Add ANF/ CNC suspension
4–19	High speed mixing
19–22	Handling and transport

Table 5
Minimum cover requirements with regards to durability of reinforcement steel according to EN10080 (all values are in mm).

Structural class	Exposure class according to Table 4.1 in EC2						
	X0	XC1	XC2/XC3	XC4	XD1	XD2/XS1	XD3/XS2/XS3
S1	10	10	10	15	20	25	30
S2	10	10	15	20	25	30	35
S3	10	10	20	25	30	35	40
S4	10	15	25	30	35	40	45
S5	15	20	30	35	40	45	50
S6	20	25	35	40	45	50	55

X0: no risk of corrosion or attack
XC1: carbonation induced corrosion; dry or permanently wet
XC2: carbonation induced corrosion; wet, rarely dry
XC3: carbonation induced corrosion; Moderate humidity
XC4: carbonation induced corrosion; Cyclic wet and dry
XD1: Chlorides induced corrosion; Moderate humidity
XD2: Chlorides induced corrosion; wet, rarely dry
XD3: Chlorides induced corrosion; Cyclic wet and dry
XS1: Chlorides induced corrosion exposed to sea water; not direct contact to sea water
XS2: Chlorides induced corrosion exposed to sea water; submerged in sea water
XS3: Chlorides induced corrosion exposed to sea water; Tidal, splash, and spray zones.

Table 6
Adjusting structural class according to applicable criterion.

Criterion	Exposure class according to Table 4.1 in EC2						
	X0	XC1	XC2/ XC3	XC4	XD1	XD2/ XS1	XD3/XS2/ XS3
Design working life of 100 years	+2	+2	+2	+2	+2	+2	+2
Strength class	≥C30/ 37	≥C30/ 37	≥C35/ 45	≥C40/ 50	≥C40/ 50	≥C40/ 50	≥C45/55 -1
	-1	-1	-1	-1	-1	-1	
Member with slab geometry position of reinforcement not affected by construction process	-1	-1	-1	-1	-1	-1	-1
Special quality control of the concrete production ensured	-1	-1	-1	-1	-1	-1	-1

completed in the early days of August 2020.

Validation tests were thereafter performed on the following dates:

2nd July 2020, 3rd–4th August 2020, 8th September 2020, 25th March 2021, 18th–19th April 2021, 11th-13th May 2021, 7th-9th June 2021, 26th-29th July 2021, and 7th-10th March 2022.

The tests consisted in filling each compartment (which, considering the volume of water entering it equal to about 70 m^3 required a whole day), leaving it full at the end of the test, and measuring the following quantities: wall deflections at different locations;.

- steel strains for the ordinary reinforcement in the first compartment (ordinary reinforced concrete);
- concrete surface strains for the walls of the second and third compartment (UHDC walls);
- steel fibers dispersion tests for the second and the third basins (UHDC walls), via magnetic inductance survey: it served as a construction quality control test;

- crack sealing observation by optical microscopy for the all compartments;
- visual inspections to monitor any sign of degradation or leaching for all the compartments.

Fig. 4. Construction steps of the third basin – (a): pre-casting the slabs horizontally, (b) cast in place the columns, (c) arranging the precast slabs vertically in their positions before casting the stiffening column.

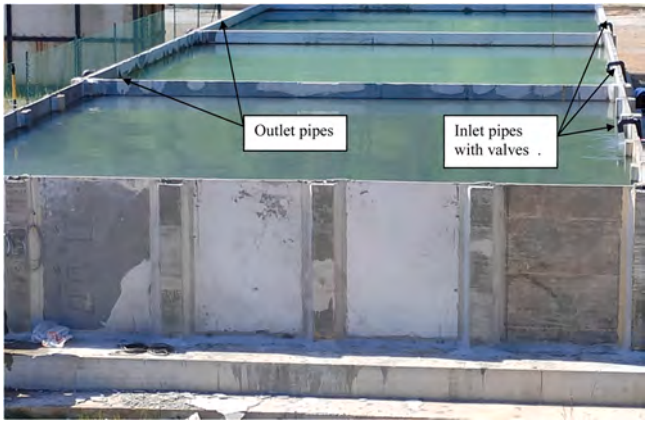

Fig. 5. The basin is completed and filled with geothermal water in its three compartments in its design structural service scenario (in forefront the buttress columns stiffening and connecting the 30 mm precast UHDC slabs are evident).

3.1. Load/water level versus horizontal displacement behavior

During the emptying/filling of the individual basin compartments, the (outward) deflections of the walls were measured using, for each compartment, nine LVDTs with 100 mm max stroke positioned as shown in Fig. 6. The nine LVDTs were distributed over three stands, which, on their way, were positioned along the walls of each compartment in such a way to capture the main behavior of the entire wall. The middle stand was positioned at mid length of the wall to capture the maximum displacements and the other two at 1/4th of the wall's length. For the third compartment, two different measuring schemes were adopted: in the 18th April 2021, and 11th May 2021 tests one stand was positioned in correspondence of a buttress and the other two at mid span of the two adjacent slabs; on the 7th June 2021, 26th July 2021, and 7th March 2022 tests, displacements were measured at mid-span and at quarter spans of one slab. Each stand carries three LVDTs: the first one is projected on the top edge of the wall, the second one is 500 mm downward from the first one, and the third one is 500 mm further downward, i.e. 1.0 m downward from the first one.

The water level was identified by referring to a measuring tape positioned and posted on the interior face of the wall of each compartment and the corresponding displacements were recorded at every 50 mm water height increment. The filling of the compartments was stopped when the water level reached 1.30 m, which is indicated as the service level of the water, in correspondence of

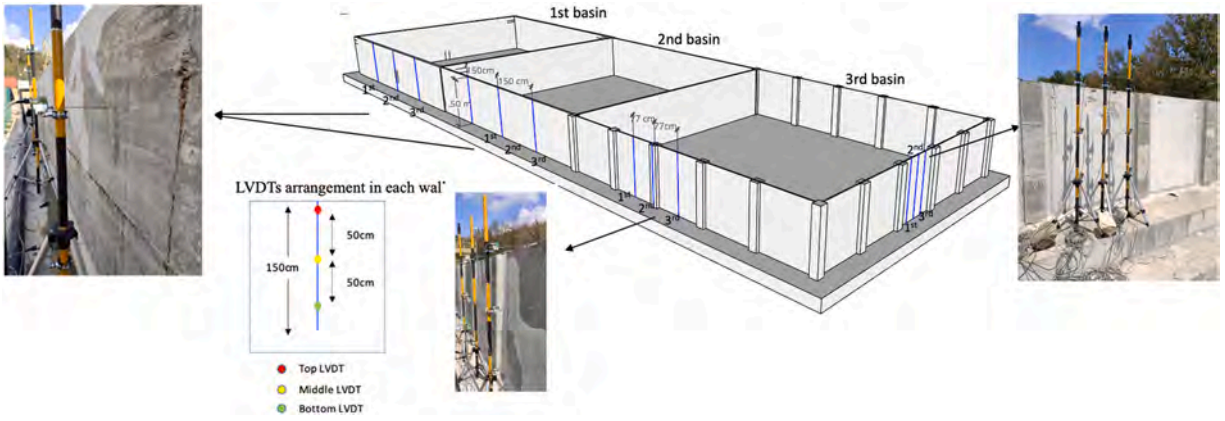

Fig. 6. Positioning of LVDTs for measuring wall deflections during basin compartment water filling tests.

the pre-installed spillage pipes.

It is worth here remarking that with the expected amount of the displacements and the size of the structures, it was very challenging to obtain the precise displacements within 0.1 mm precisions for the third compartment and 1.0 mm precision for the first and the second compartments. Moreover, the effects of the weather fluctuations and direct sunlight on the thin UHDC walls during the test time, which minimally took five hours to be completed, excluding the instrument preparation and connection time, resulted in fluctuation of the results for some performed tests. However, the repetition of the tests in different seasons of the year and the corresponding measurements helped to refine the fluctuation of the results; the most repeatable results have been reported in the current study to be considered as the most reliable and representative measurements.

3.1.1. First compartment (ordinary reinforced concrete basin)

The water level vs. deflection results obtained from filling the first compartment are shown in Fig. 7**.** The results were processed to show how the displacements of the selected points evolved as the percentage of the water levels inside the basin increase from 0% to 100% (130 cm). In addition, an elastic numerical analysis of the behavior of the whole wall, discretized through plate elements and with boundaries considered either as fully fixed or simply supported has been performed, whose results are also reported in the graphs in Fig. 7.

It is worth first of all remarking that some lack of symmetry between the left and right quarter wall length measurements started occurring from filling level equal to about 30% of the full service condition (approximately 400 mm water); this could be explained by the closeness to the right quarter wall-length pole to previously formed shrinkage cracks (see Section 3.4.1) which may have affected the local stiffness response. Anyway displacements always remained below the elastically calculated ones for the fully fixed edges obtained from FEM analysis of the structure.

On the other hand, for the mid-wall length displacements, the comparison with elastic numerical analyses indicates that the tip point overpasses the maximum displacement corresponding to the fully fixed edge assumption when the water level exceeds 40% of the basin capacity (about 500 mm). This behavior can be justified by the restrained shrinkage cracks observed at the bottom of the wall and reported in the following sections, which may have weakened the wall to foundation connection making it to work as pin support also could be due to the water mass wave induced by the feeding pipes.

3.1.2. Second compartment (UHDC continuous thickness wall)

The same scheme followed above has been employed to process the results of the tests carried out for the second compartment which is characterized by a 60 mm thick cast in place UHDC wall (Fig. 8a–c respectively for the displacements measured at 1/4th of the wall length close to the first compartment side, at mid-length, and at 1/4th of the wall length close to the third compartment side)**.**

The results show that the wall is generally performing as a slab fully fixed along three edges and free along its top edge; it can be in fact observed that the maximum displacements captured from all the stands are laying within the envelope of the results obtained from a linear elastic FEM analysis for the slab with fixed edge boundary condition. Nonetheless, when the water approaches its maximum level, the left side close to the first basin tends to significantly deform, more than the elastic finite element prediction values.

Referring to Fig. 1, it can be seen that the corner close to the third compartment (and hence to the pole where displacements shown in Fig. 8c where recorded) was monolithically casted with the transverse wall (i.e. the wall dividing the second and the third compartments). On the other hand, the corner close to the first compartment, which is close to the pole where the displacements shown in Fig. 8a were recorded, was not monolithically casted with the transverse wall, which was made of ordinary concrete and divides the first compartment from the second one. This created uneven boundary conditions for the wall which resulted into higher displacements to occur near the left side.

3.1.3. Third compartment (30 mm thick UHDC slabs stiffened by 200 × 200 mm^2 cast in place UHDC columns)

According to the processing scheme explained in the previous sections, the displacement readings from the LVDTs in the third basin

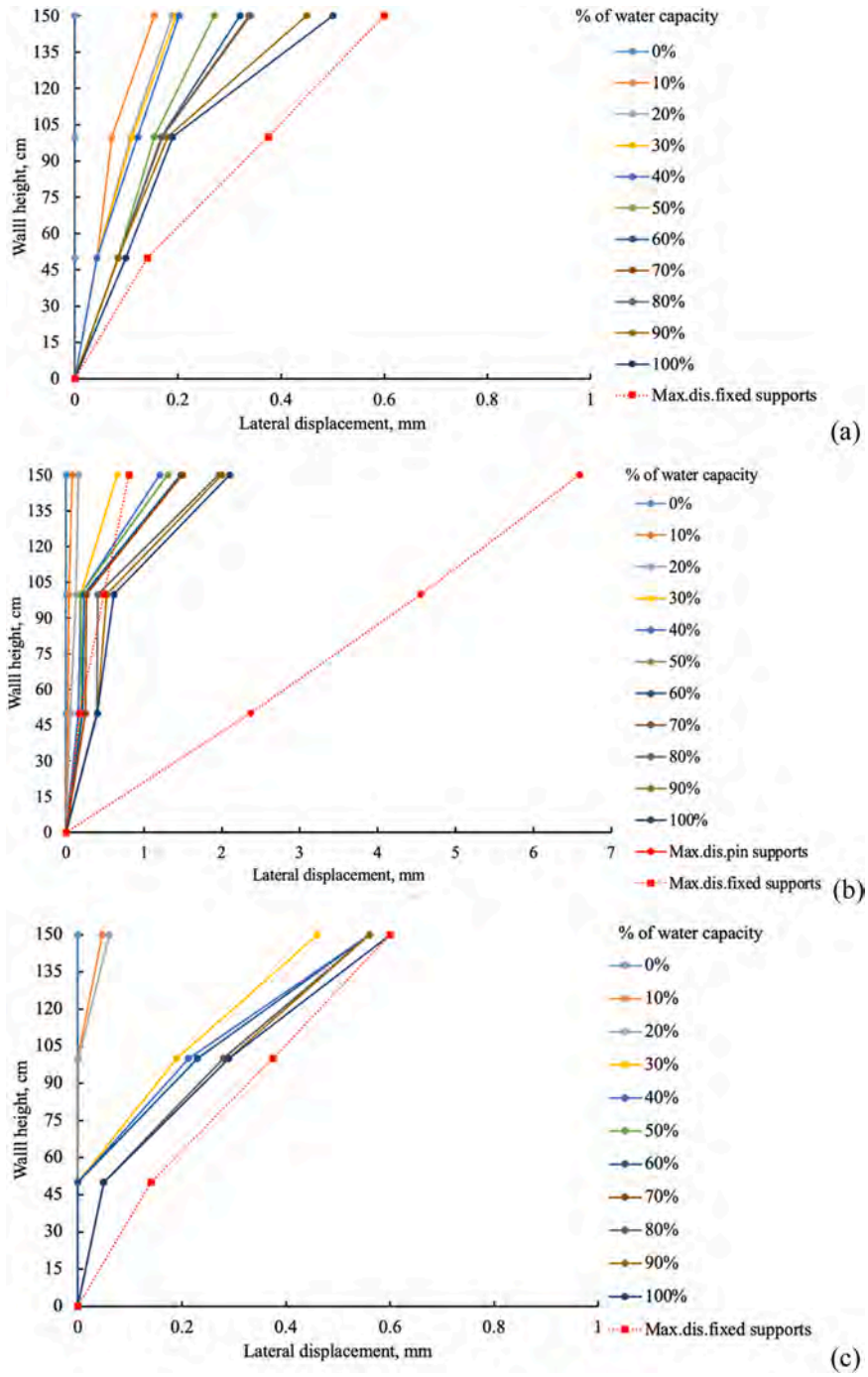

Fig. 7. Water level vs. displacements for the first compartment: (a) left quarter-wall length; (b) mid-wall length; and (c) right quarter wall length.

were taken from two different layouts. In the first layout, which is aimed to capture the global behavior of the composite wall, the poles with their three LVDTs were distributed on the middle of two adjacent slabs and the column between the slabs, the results of this layout are displayed in Fig. 9. The second layout, on other hand, is aimed at capturing the local deformation mechanism of each single slab, with the poles positioned at mid-span and at the left right quarter spans of the selected slab, the related results of this layout are shown in Fig. 10a–c.

In the same figures, the results of linear elastic numerical analysis obtained by FEM analysis with fixed and pin boundary conditions are also shown in Figs. 9 and 10. The results of the middle stand, laying very well within the envelope of numerical analysis results for fixed edges, clearly confirm the two-way slab system behavior. However, the results from the sides stands have small deviations when

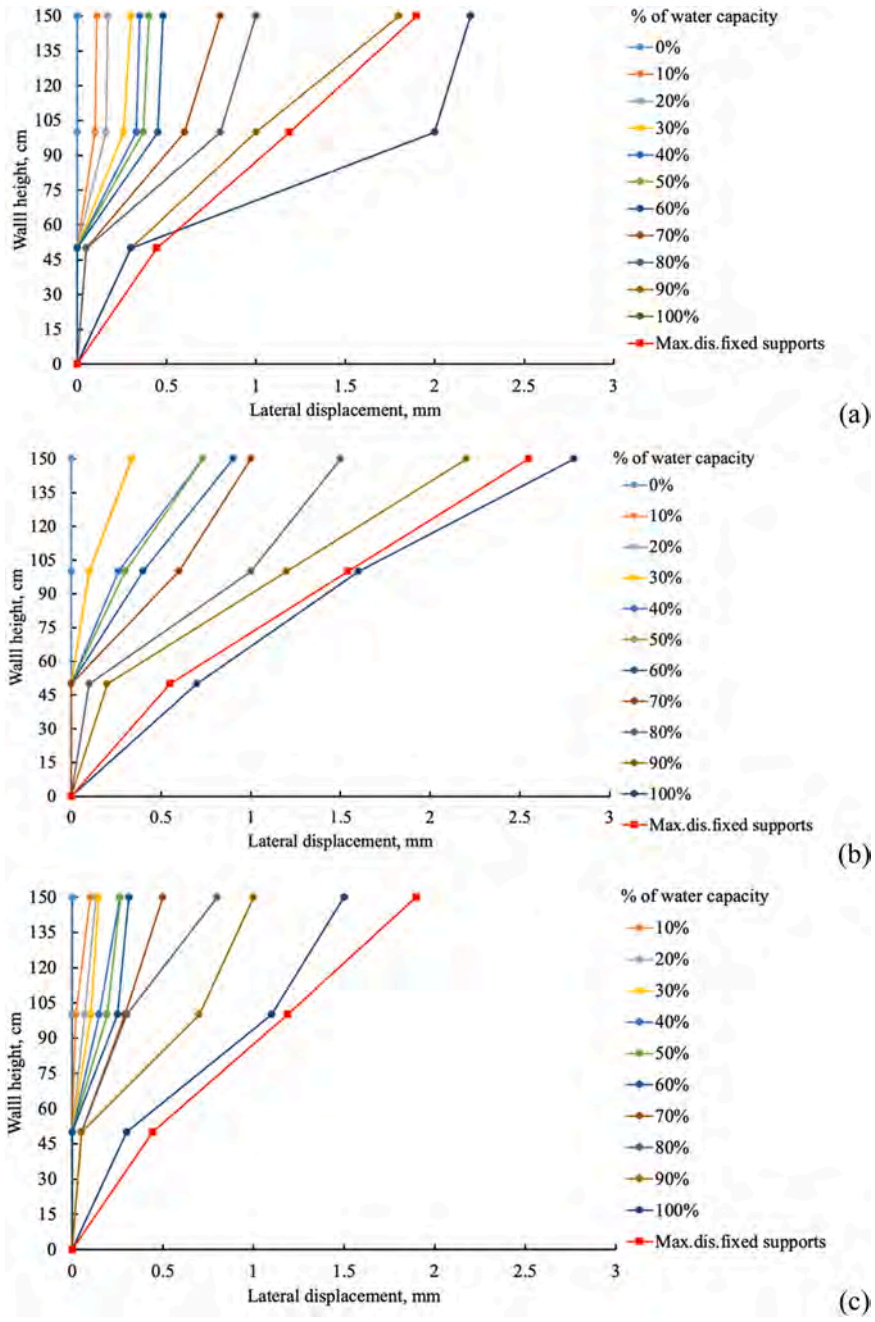

Fig. 8. Water level vs. displacements for the second compartment: (a) left quarter-wall length; (b) mid-wall length; and (c) right quarter wall length.

the water approaches its maximum level. This deviation could be attributed to the edge boundary conditions where the slab is connected to the cast in place UHDC columns, which experienced some displacements at maximum water level as shown in Fig. 9b. It can be noticed that the maximum reading from the middle slabs pole is around 0.5 mm which agrees with the numerical results. However, the readings from the side poles is experienced 0.1 mm more which is the same displacement captured by the column at the maximum water level. Finally, the behavior of the middle pole of the slab in Fig. 9 clearly shows the two- way behavior which is laying perfectly with the expected numerical analysis.

Summarizing the results and illustration of the different displacement measurements, Fig. 11 is schematically showing the position and the deformed shaped of each wall, together with the results of a yield line analysis, reported in detail in [34] for the comparison purposes. The UHDC columns successfully stiffened the walls of the third basin, shifting the global response mechanism towards a local one, which in turns brings more redundancy to the system. The not monolithically casted joints in the second wall affect the symmetry

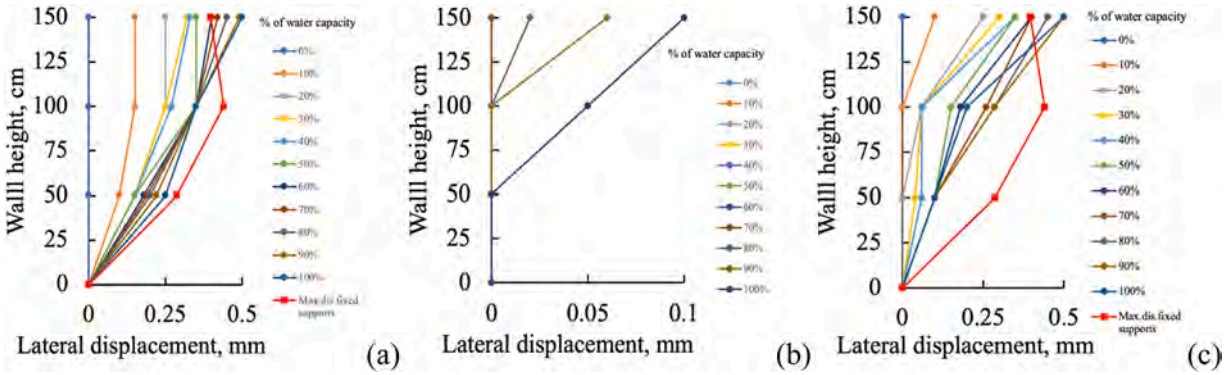

Fig. 9. Water level vs. displacements for the third compartment (first lay-out) for two adjacent slabs (a, c) and the 200 × 200 mm^2 cast in place UHDC column between them (b).

of the displacement response of the second wall, whereas the restrained shrinkage cracks affected the stiffness of the first basin walls (whereas they did not evidently appear in the second wall, likely because of the effective controlling action provided by the fibers).

3.2. Load/water level versus strain gauges installed on steel bars and concrete surface

During the construction of the first compartment, strain gauges were installed on the steel bars at different positions to capture the steel strain during filling of the basin. Strain gauges on the concrete surface of the second and third compartments were also installed upon the completion of the basin construction. Fourteen strain gauges were installed on the surface of steel bars, labeled from 1 to 14. To avoid lack of information due to accidentally loss of one strain gauge during pouring of the concrete, two strain gauges were installed in each position, i.e. strain gauges 1 and 2 correspond to the same position as well as 3 and 4 and so on. Twelve concrete strain gauges were installed on the surface of the second compartment wall, oriented both horizontally (HA, and HB), and vertically (VA, and VB) along the height of the wall. One of the slabs and columns of the third compartment were also provided with concrete strain gauges. The slab was provided with two vertical strains gauges on the middle (V3) and on the bottom (V4), two diagonal strain gauges on the bottom of the slabs D1 and D2 and four horizontal strain gauges (O1-O4) at mid height (mid-span and quart spans) and at mid span at the top edge of the slab. The column was provided with two vertical concrete strain gauges, V1 at middle of the column and V2 at the bottom of the column to capture the longitudinal strains. The schemes in Fig. 12 show the positioning of all the strain gauges as detailed above.

3.2.1. First basin reinforcement strain

Fig. 13a and b show the strains measured at the surface of the steel bars reinforcement running in the vertical and horizontal directions respectively. The strains were measured as the water was filling the basin with 50 mm increments up to 1.30 m which is assigned as the service water level. All the measured strains are lower than yielding strain of the steel bar reinforcements, which matches with the global response of the compartment wall substantially remaining in the elastic regime, as confirmed by the analysis of the displacement response in Section 3.1.

The strain gauges #11 and #12 which are located at 700 mm from the bottom of the wall is picking more longitudinal strain as compared with the other vertical ones located at the bottom, which could be due to second effect deformation of the wall that is more pronounced when approaching the center of the wall. For the strain gauges posted on the horizontal bars, the reading is ranging from 100 micro strain to 350 micro strain which could be due to the difference in the rigidity of the joint connection, where the steel gauges are posted.

3.2.2. Second basin concrete surface strains

For the walls of the second compartment, concrete strain gauges with a 100 mm base length were positioned along the vertical and horizontal directions as illustrated in Fig. 14a. Strain measurements from vertical and horizontal strain gauges are also reported in Fig. 14b and c respectively.

The obtained measurements indicate that all the strains are equal to or lower than 300 micro strain, where the vertical strain close to the middle of the wall have registered the highest values. The same observation from the horizontal strain gauges, where the strain gauges close to the middle have registered the highest values of 250 micro strains.

These values, for the material employed in the construction of the basin compartment, which has a first cracking tensile strength equal to 6–8 MPa, a stiffness of around 40,000 MPa (tensile strain at first cracking equal to about 150–200 micro strains) and a tensile strain capacity of about 5 × 10^{-3} may indicate that, along the continuous filling of the basin, the materials enters its micro-cracking tensile strain hardening regime. The stress redistribution capacity which characterizes this stage of the material tensile behavior may also be noticed from the fact that (Fig. 14c) the measured strains in the horizontal direction, and to some extent also those along the vertical one, show after an initial growth, a quasi-constant trend. This may be an indication of the aforesaid stress redistribution

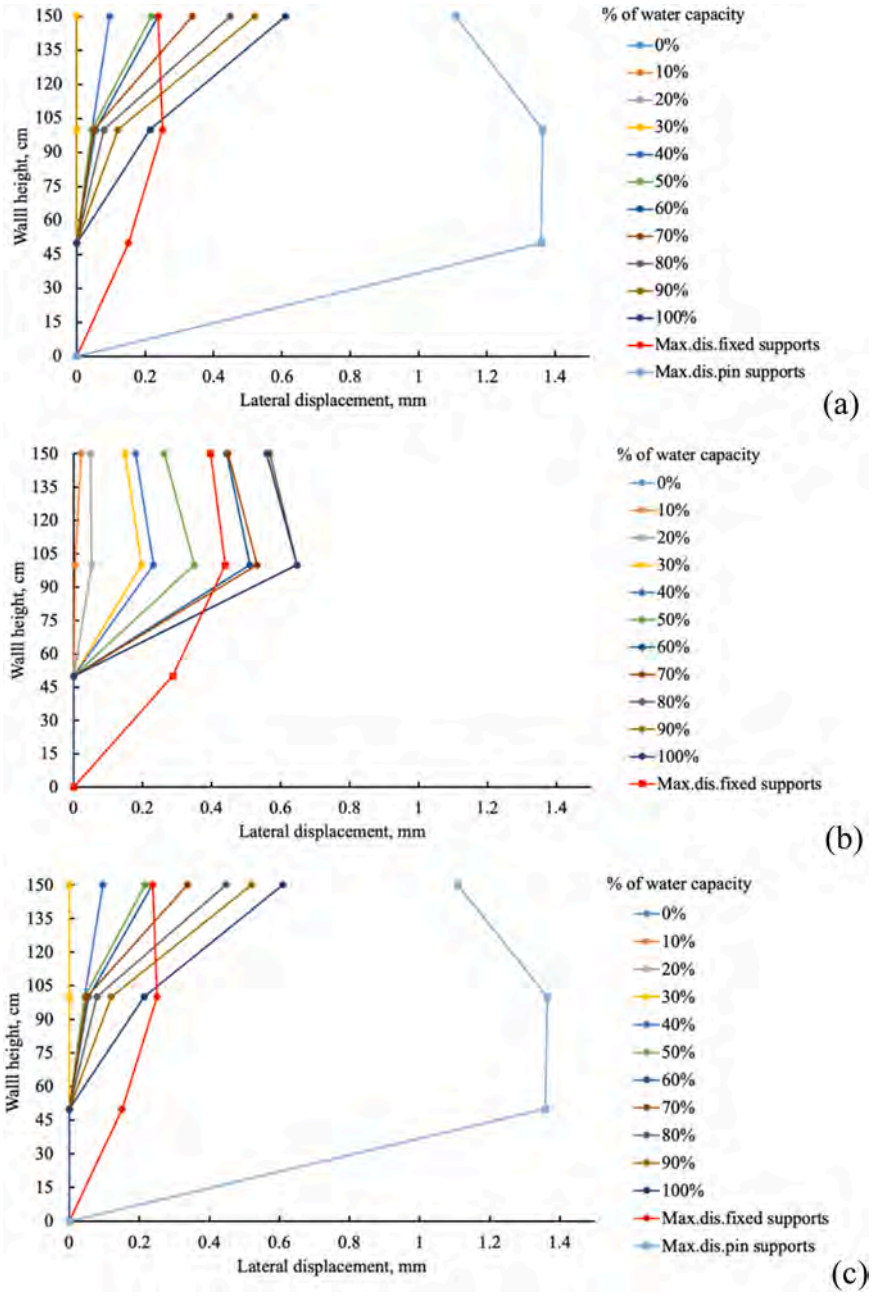

Fig. 10. Water level vs. displacements for the third compartment (second lay-out): (a) displacements at left side stand; (b) at middle stand, and (c) at right side stand.

which implies the progressive involvement of the zones at the vicinity where the strain gauges are placed as long as the static load of the compartment walls proceeds with the increasing level of the filling water.

3.2.3. Third compartment concrete surface strain

For the third compartment, strain gauges with a 100 mm base length were installed on the surface of one UHDC slab and of the supporting column. As shown in Fig. 15a, the column was provided with only two vertical strain gauges, whereas the slab has horizontal, diagonal, and vertical strain gauges. The measurements from vertical and horizontal/ diagonal strain gauges are reported in Fig. 15b and c respectively. The vertical strain gauges showed the least values of strain 100 micro strains, whereas the diagonal strain gauges and the top horizontal strain gauges registered the highest values of 250 and 400 micro strain respectively. These are respectively lower and absolutely comparable with the values measured for the second compartment, which consisted of 60 mm thick

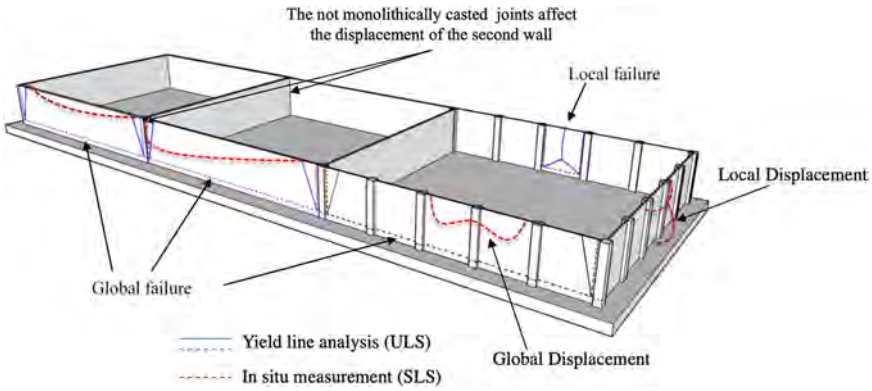

Fig. 11. Global illustration of the global displacement response for all the compartments from water filling tests.

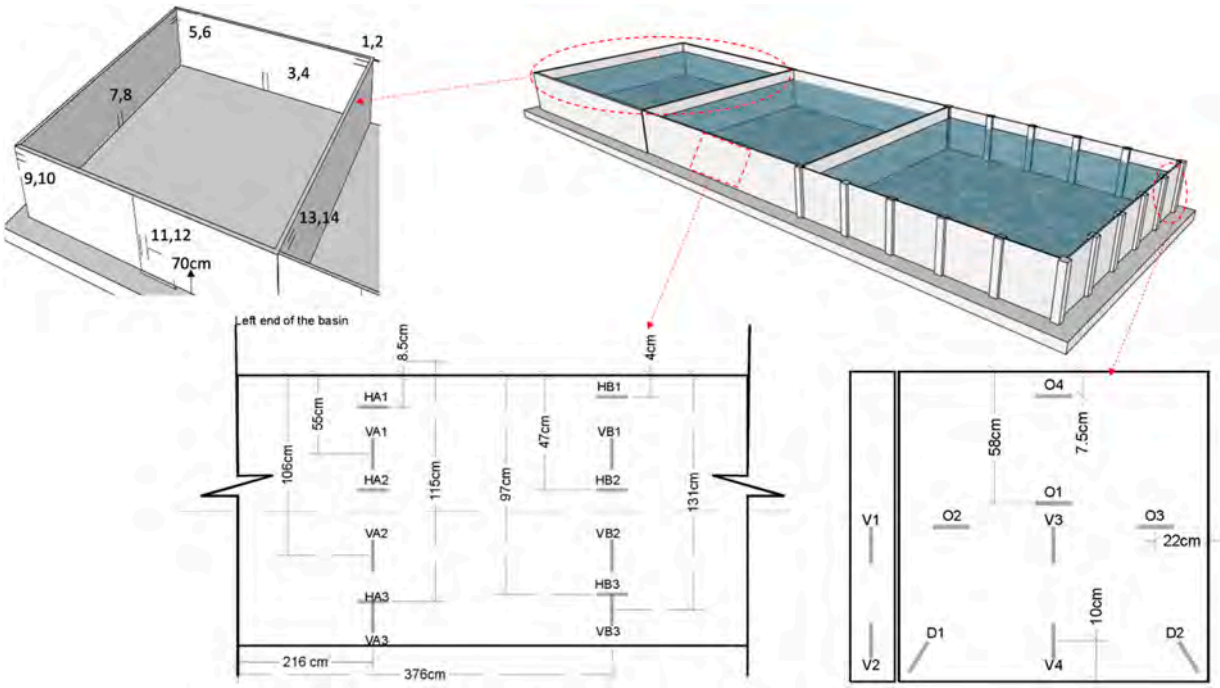

Fig. 12. Positioning of strain gauges on the different compartments of the basin.

walls, and confirms the reliability of the precast 30 mm thin slab stiffened by column buttresses structural concept implemented in the third basin. As for the numerical values of the measured strains, the same statement stated previously with reference to the second compartment hold.

According to the EN-1992—Part 3 [35], where strain limits for liquid retaining and containment structures are set depending on the leakage requirements, the tightness class is classified from 0 to 3. Class 1 tightness indicates that some amount of leakage is permitted, such as surface staining and damp patches. In this case, the strains under service condition have to be limited to 0.00015 mm/mm (150 micro strains), which is very close to most of the strain levels measured under service actions for Basin 2 walls and Basin 3 under the service load level.

As a matter of fact, considering that no leakage was observed on the walls of both the second and third compartments, for the corresponding measured values of strains, which are somewhat higher than the one permitted by EN 1992–3, it can be reasonably argued that for the UHPC/UHDC materials employed in this pilot structure the permitted leakage strain limits, calibrated on ordinary reinforced concrete, might be revised. This can favorably exploit the signature multiple cracking which features the post-first cracking and strain hardening stage of the material behavior where, as said, the damage is spread into a number of tightly spaced and narrowly opened micro-cracks instead of being localized into a single wider opened crack.

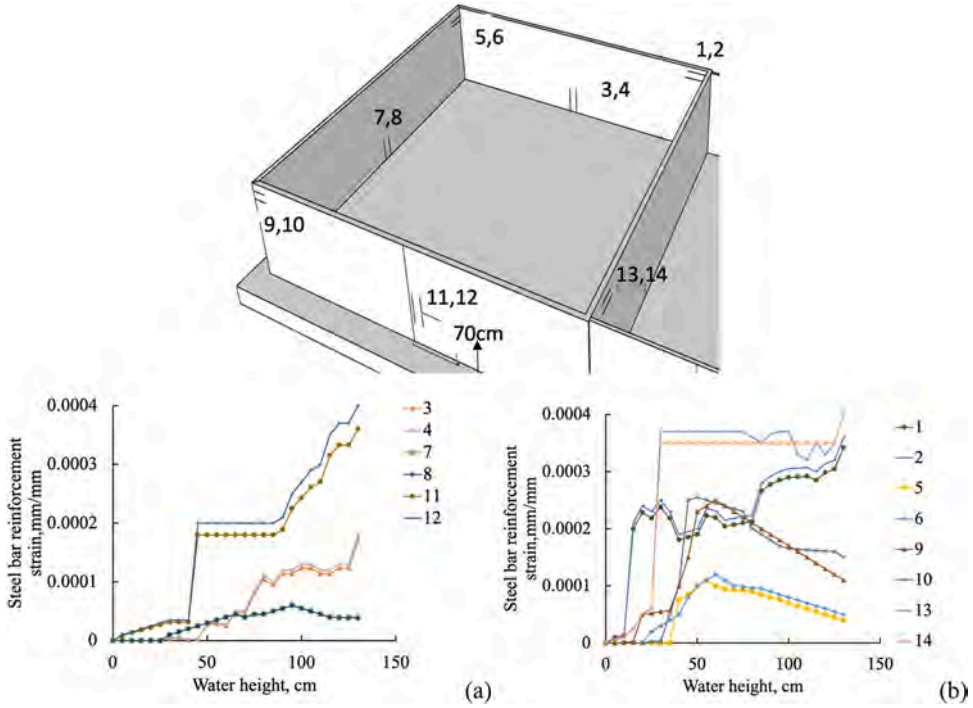

Fig. 13. Illustration of water level- steel bar strains for the first basin, a- strains from vertical bars, and b- strains from horizontal bars.

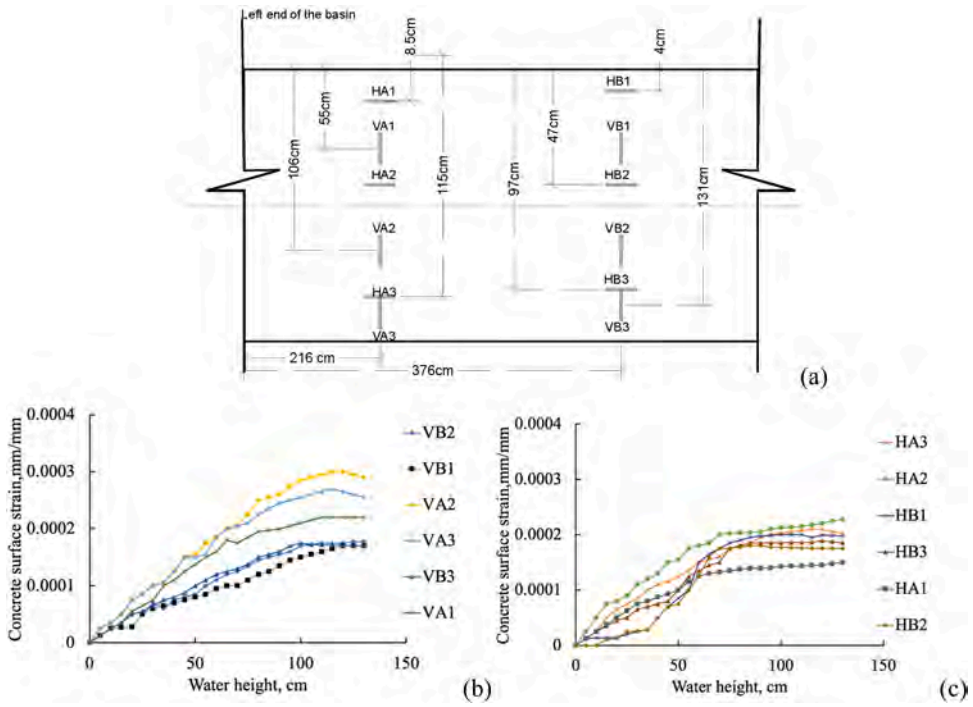

Fig. 14. Concrete surface strains vs. water level for the second basin: (a) positioning of strain gauges, (b) strains along the vertical direction and (c) strains along the horizontal direction.

3.2.4. Analytical model to predict the behavior of the walls at service water level

In order to predict the behavior of the basin walls, non-linear sectional analysis of the basin wall was performed as shown in Fig. 16, where the basin wall was modeled as a cantilever beam (1.0 m width) fixed at the bottom to the foundation. Since the proposed

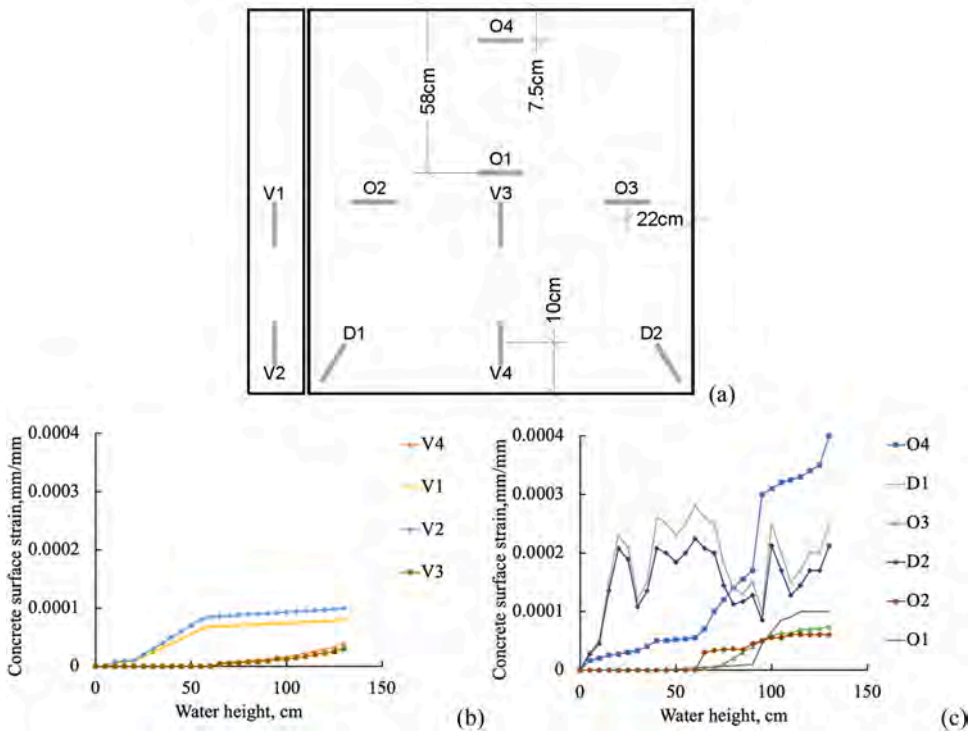

Fig. 15. Concrete surface strains vs. water level for the third basin: (a) positioning of strain gauges, (b) strains along the vertical direction and (c) strains along the horizontal/diagonal direction.

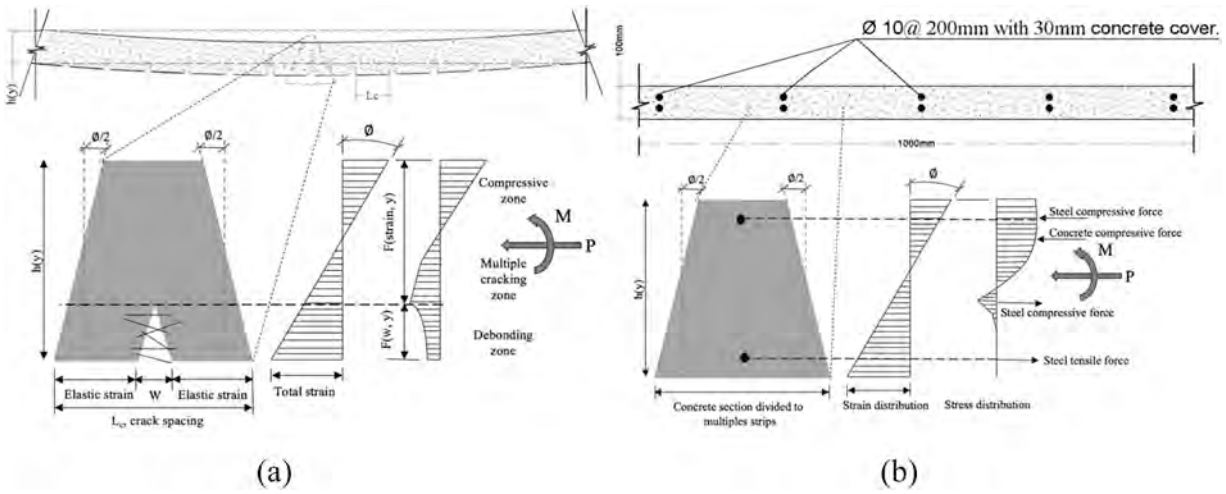

Fig. 16. Sectional analysis of the basin walls, a- UHDC section, and b- reinforced concrete section.

sectional analysis was already used to predict the service life of the basin [36], it is necessary to validate it with the on-site strain and displacement measurements and vice versa. The displacement-water height response of all the three compartments has been analysed and compared with the onsite measurements as reported in Fig. 17 for comparison with elastic numerical analysis previously mentioned and the on-site measurements. In addition, in this paper, the steel strain of the first basin compartment, as well as the concrete surface strain of the second (considering a 1.0 m wide cantilever wall strip) and the third compartments (in this latter case reference has been made to the column for which a cross sectional analysis could be reliably applied) have been extracted from the model and compared to the on-site measurement as shown in Fig. 18. The nonlinear analysis reasonably agrees with the measured ones for the second and the third basin. However, for the first basin, the onsite measurements exhibited lower stiffness, which could be due to the restrained shrinkage cracks observed at the bottom of the wall.

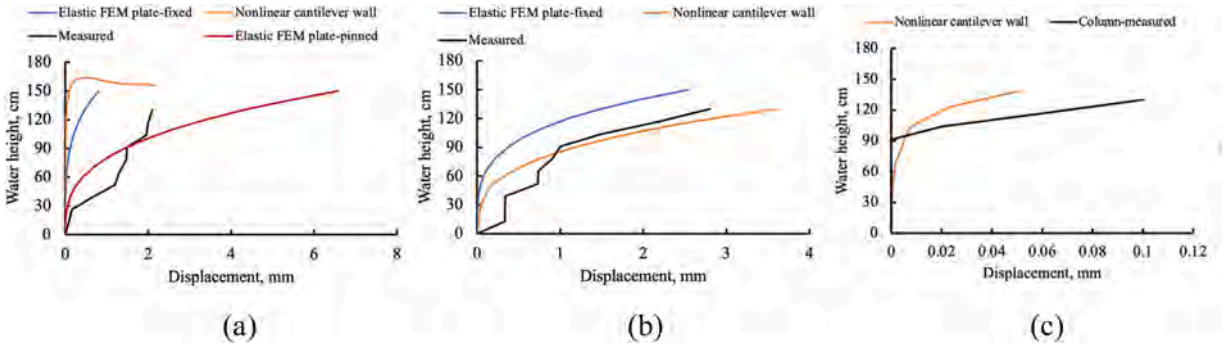

Fig. 17. Comparison of nonlinear analytical analysis, and numerical elastic analysis vs measured water level- displacements: a – first basin; b- second basin, and c- the third basin column.

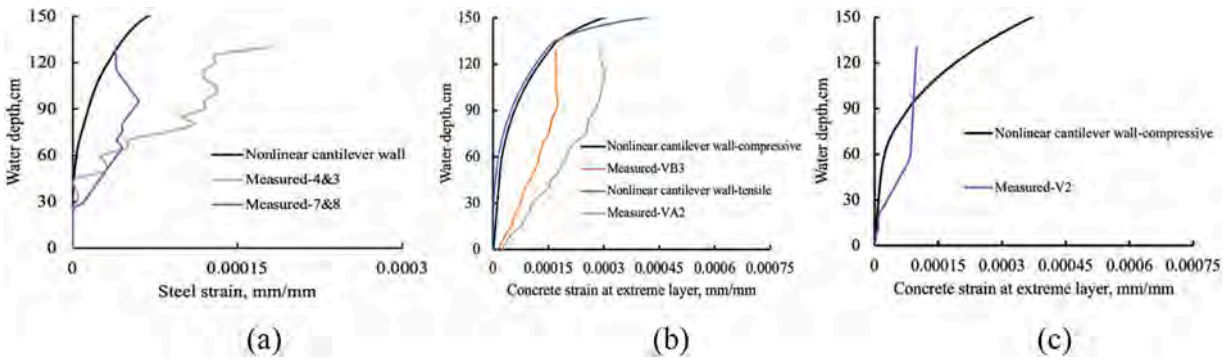

Fig. 18. Comparison of nonlinear analytical vs measured water level- strains: a - strain of the internal vertical steel bar reinforcement; b- strain of the concrete for the second basin wall, and c- strain of the concrete for the third basin column.

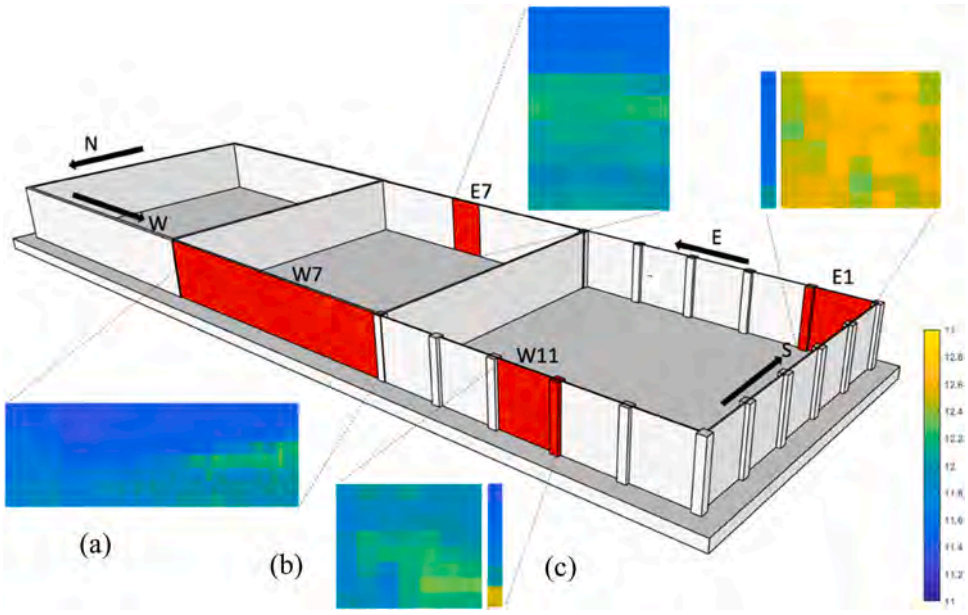

Fig. 19. Steel fibers distribution survey: (a): cast in place 60 mm UHDC wall, (b): precast 30 mm UHDC slab, and (c): cast in place 200 × 200 mm^2 UHDC column.

With reference to the strain measurements, as compared to nonlinear analysis of the fixed wall, they show higher values. It should be kept in mind that the on-site measurements were registered at a very slow loading rate combined with the long thin wall and the weather effects which could result in higher strains than the ones obtained from the analyses.

3.3. Steel fiber dispersion tests for the second and third compartments (UHDC walls)

Steel fiber dispersion was surveyed for specific precast and cast-in-place UHPC/UHDC elements, as illustrated in Fig. 19 below. The magnetic method proposed and validated by Ferrara et al. [11] was adopted in this survey for its robustness and easiness to handle at the job site. The method uses a probe with sensors spaced at 160 mm, which create a magnetic field, sensitive to the magnetic properties of the steel fibers aligned within its domain, thus resulting in variation in the measured inductance when the sensor is placed in contact to the surface of the basin wall, along a different specified direction. The results of the measurements were recorded via a MATLAB script. A detailed description of the method and its calibration can be found in [11,37,38].

Results qualitatively plotted in Fig. 19 indicate that fiber dispersion is quite homogenous for the pre-cast elements (b), which were casted horizontally. On the other hand, for the cast-in-place elements wall (a) and the column (c), some settlement of the steel fibers occurred in the top layers; this observation implies that the precast application of UHPC should be preferred, particularly for vertical structural elements where vertical casting may jeopardize the distribution of the steel fibers and affect the performance of the structural elements as clearly illustrated in Fig. 20 even prior to the application of the load where shrinkage issues can be involved as it will be addressed later. Nonetheless, comparing the two cast in place elements, the wall thickness was 60 mm and the column 200 × 200 mm^2 divided by the adjacent slabs into two parts, each part would be 200 × 80 mm^2. It's clear from the magnetic survey that the column suffered from higher segregation than the wall. This can be explained considering that while the columns casting can be done with one casting batch, the long wall was casted in multiple batches, the interval time between each batch being around half an hour. Moreover, the casting of the long wall was stopped half-way during the mid-day, and resumed one hour later. On the other hand, and for the case of the wall, the flowability of the concrete along the horizontal direction is pushing the steel fiber away from the casting point (Fig. 20) and make the fibers to concentrate away from that point as clearly proven by the magnetic survey of the entire side of the second basin Fig. 19a, where the casting point is very evident formed like a conical shape where steel fiber is pushed away.to the side of the wall.

In order to calibrate the sensor reading to the actual steel fiber content, ten UHPC slabs of 1.65 m × 1.5 m× 0.033 m similar to the precast elements used in the third basin were randomly chosen and surveyed using the same sensor and methodology described for the pilot. The qualitative results shown in Fig. 21 below were normalized based on the volume of the scanned slabs and the amount of the steel fibers incorporated in the design mix, Table 2, then each magnetic sensor reading from the grid of the slabs was correlated with the amount of steel fiber in terms of kg/m^3. Based on the results shown in Fig. 22, it was concluded that the sensor reading of 12.38 is equivalent to steel fiber content of 120 kg/m^3 which is the design value of the UHPC mix. Also it can be noted from the statistical analysis displayed in Fig. 22 that most of the surveyed cells are reasonably agreed with the design steel fiber content of 120Kg/m^3.

3.4. Crack healing/sealing inspection tests for all basins

Once the three compartments had been completed and before entering their service life, a crack survey was carried out. The cracks were scanned with microscopic device and selected image spots were coded.

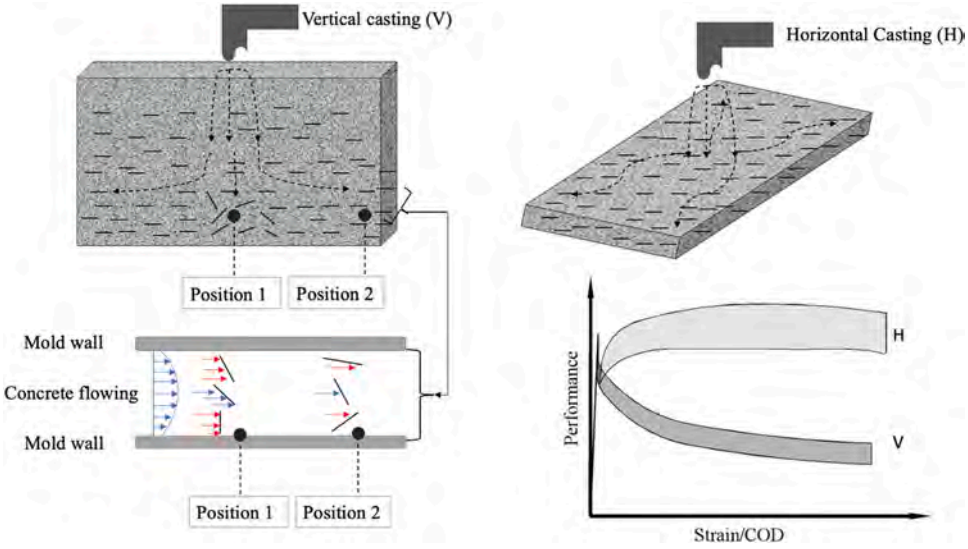

Fig. 20. Illustrating the mechanism and the effect of the vertical and horizontal UHPC casting.

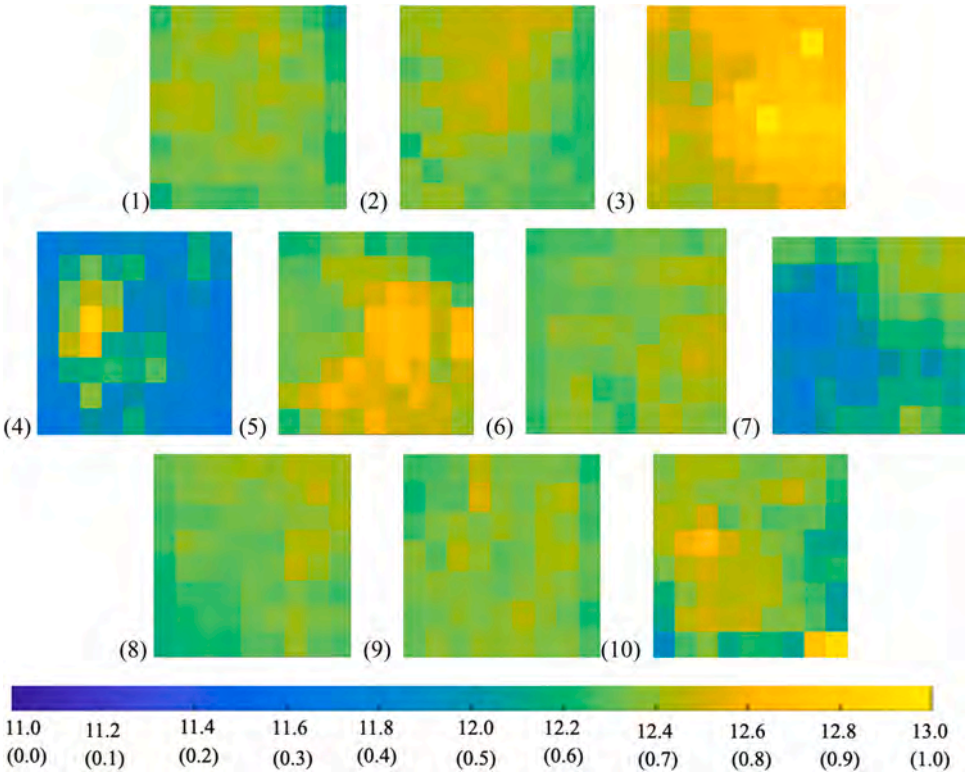

Fig. 21. Steel fibers distribution survey for the horizontal casting of UHDC slabs (values in μH).

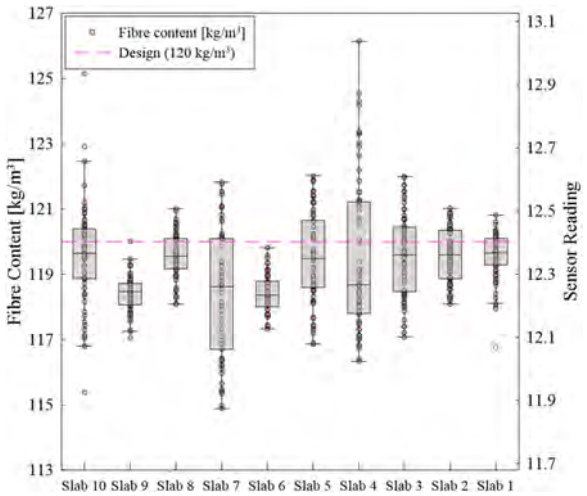

Fig. 22. Correlating the sensor reading with steel fiber content.

3.4.1. First compartment crack width survey

The survey for the first compartment was performed as explained in Fig. 23. Several longitudinal cracks have been noticed in the first compartment. These cracks are believed to have formed due to the restrained shrinkage. Repaired action was taken for cracks larger than 0.3 mm. Cracks narrower than 0.3 mm were not repaired (highlighted in red), whereas microscopic pictures have been periodically taken to evaluate their self-healing after the compartment entered its service phase. The autogenous crack sealing was observed for narrow cracks at the top of the wall, where the measured crack widths were lower than 0.3 mm [39,40], Fig. 24. The healing/sealing was efficient due to the implementation of the crystalline admixture in the mix of the first basin.

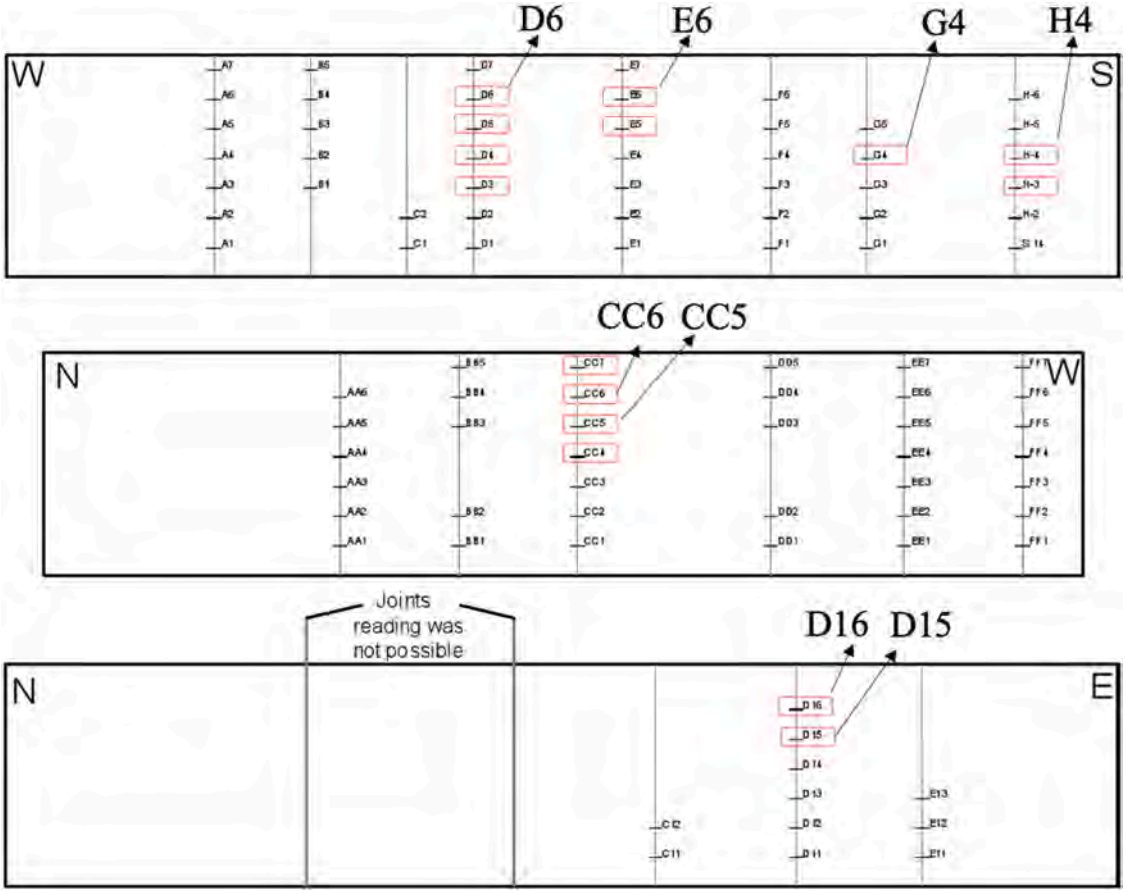

Fig. 23. Crack length and width mapping of the first basin.

3.4.2. Second compartment crack width survey

The second compartment of the tank, with UHDC cast in place walls, also exhibited some hairline cracks that appeared only in the top edge of the wall. The uneven distribution of the steel fibers in this wall described in Section 3.3 resulted also into higher proneness to drying shrinkage cracking. As a matter of fact, these cracks, spaced about 250 mm, extend about 500 mm downward from the top edge of the wall, which corresponds to the depth of the zone where a lack of steel fibers was detected through a non-destructive survey (Fig. 19-a). During the filling of the basin these cracks picked some moisture and, as of August 2021, they are completely sealed, except one vertical crack extended to the bottom, which is still being monitored to evaluate its self-healing progress as highlighted in red in Fig. 25. The latest visits to the pilot have confirmed the sealing of these cracks as detailed in Fig. 26 for the designated cracks.

Restrained shrinkage ring tests according to ASTM C1581 were performed on the same concrete used for the second basin Fig. 27. The purpose of the test is to confirm the hypothesis that the observed cracks in the top part of the wall are due to restrained shrinkage strain. Therefore, three different steel volumes were incorporated in different batches to foresee the steel fiber distribution effect on the restrained shrinkage strain: XA-CA, and XA-CA+CNC, i.e. matrices without nano-materials and with nano-cellulose were used respectively and both without steel fibers, XA-CA-50%SV, and XA-CA-100%SV, where matrices incorporated 50% and 100% steel fiber fraction of the amount mentioned in Table 2. The concrete mixes that do not contain steel fibers cracked after 11 and 14 h for specimens without nano-materials and with nano-cellulous respectively, Fig. 28a, where the strain on the steel rings reached 15 micro strain. On the other hand, specimens with half and full amount of steel fibers content did not experience shrinkage cracks after reaching 100 micro strain in the steel rings, Fig. 28b. It is worth mentioning that the tests on specimens with full amount of steel fibers were terminated earlier than for specimens with half the fiber content to avoid the issue of the demolding from the steel rings. The test results confirm the onsite observations of the second wall, where the lack of steel fiber in the top part fostered the restrained shrinkage crack to occur.

The solution adopted for the third compartment, where the walls were made by precast UHDC slabs, revealed no shrinkage cracking problems as noticed for other basins. It is interesting to point out that after one year of being in service, some degradation has been noticed in the first basin, where leaching in immersed concrete layers was observed during filling the basin as shown in Fig. 29 right, where also some surfacing sand particles are shown which can be easily removed from the surface of the wall. On the other hand, this did not appear in the second nor the third basin, where the UHDC materials were used Fig. 29-left. The main reason for the leaching is the decrease of the pH value below the stability limits of cement hydrates, Table 1: as the acids attack concrete, calcium decomposes to

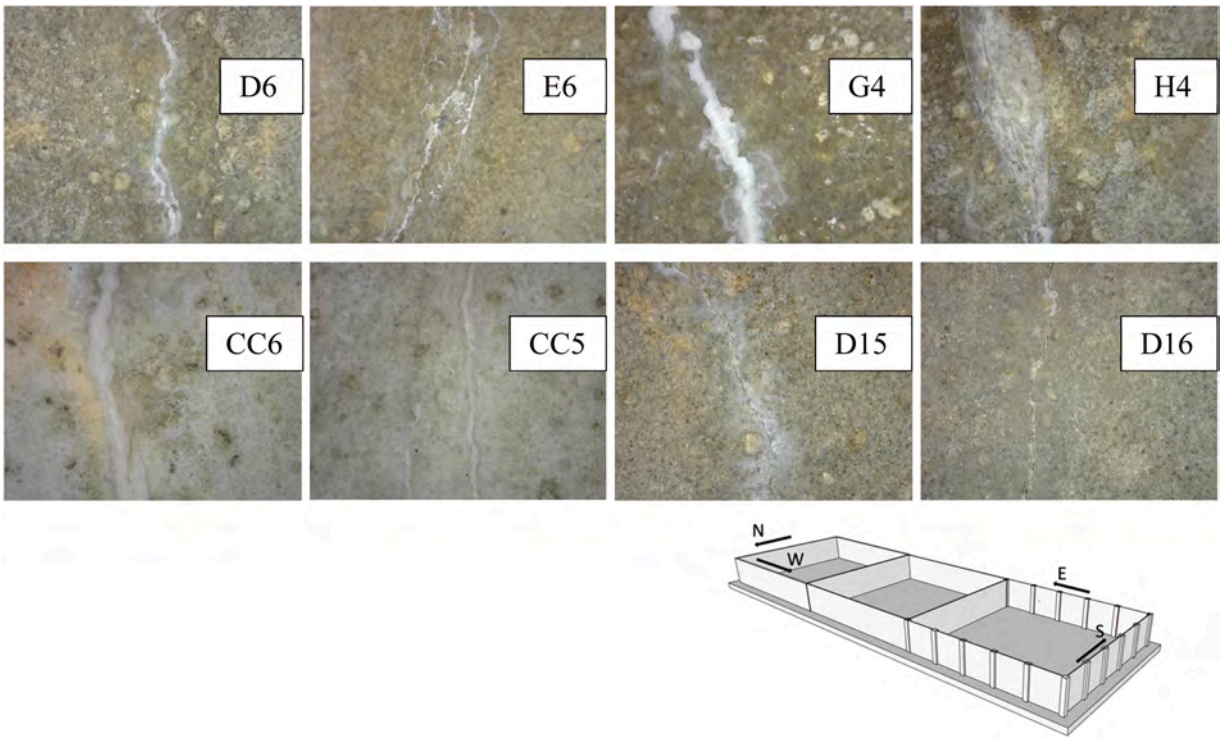

Fig. 24. Crack sealing/Healing for the designated cracks of the first compartment.

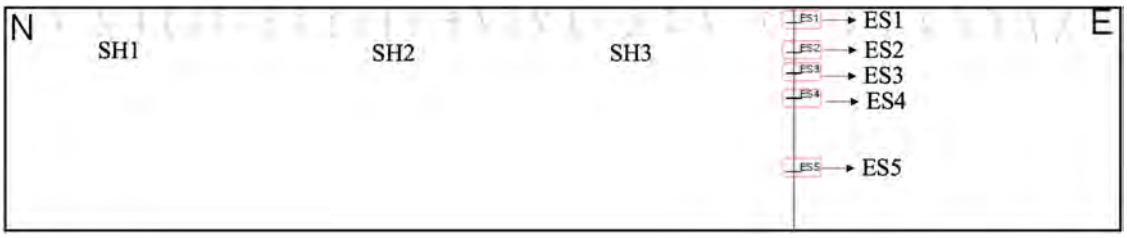

Fig. 25. Crack length and width mapping of the second basin wall.

amorphous hydrogel that can be washed out by the water enclosed in the basin, which is clearly evident in Fig. 29-right. The progression of this mechanism can lead to scaling of the section and mechanical stresses which eventually make the basin as structurally deficient.

4. Conclusions

In this paper the results of validation tests are reported of a pilot structure, being a basin for the cooling of geothermal waters, cast with advanced cement based materials developed in the framework of the Horizon 2020 project ReSHEALience (GA 760824). The basin measures 22.5 × 7 m in plan and have been built with different solutions, implying the use of ordinary reinforced concrete as well as of both cast in place and on-site precast Ultra High Durability Concretes developed in the project, the last solution allowing for up to about 70% volume material reduction as compared to the first one. The tests allowed to validate on the site the performance of the materials and also to derive useful considerations about the reliability of the design assumption and of the construction process which can be as hereafter summarized.

– Regarding the connectivity between precast UHDC elements or casted in other different time, as per the structural response, the boundary conditions for basin 2 and 3 revels very good performance that reasonably lies within the assumption of being continuous supports or fixed supports at the base or with adjacent elements. For connectivity of the wall with foundation, the UHDC elements was excellent, no signs of leakage or restrained shrinkage crack observed. The same holds for the third compartment, where the UHDC slabs connected to each other by cast in place columns experienced no leakage.

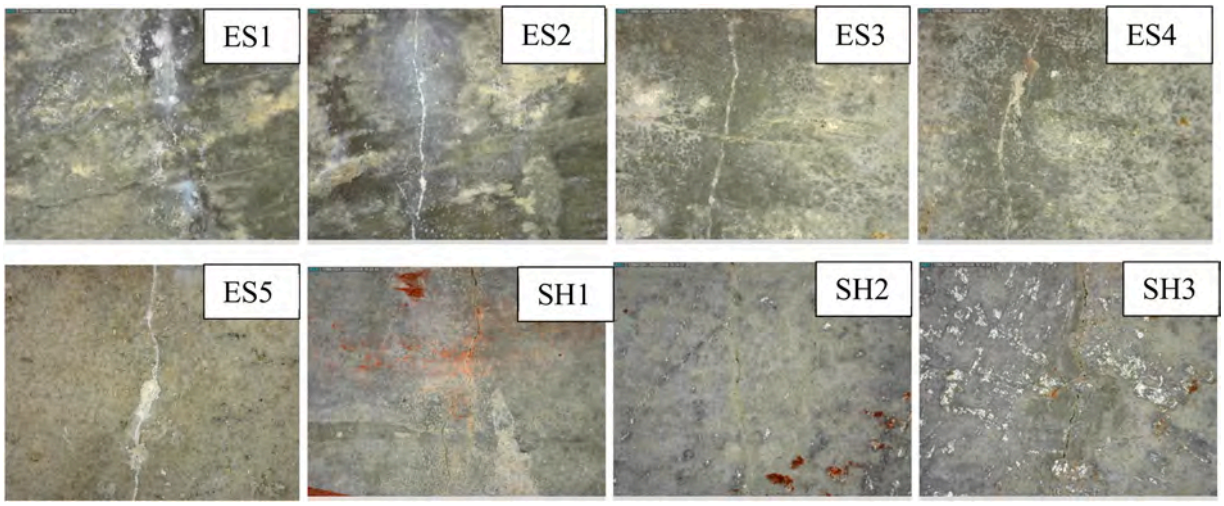

Fig. 26. Crack sealing/Healing for the designated cracks of the second basin.

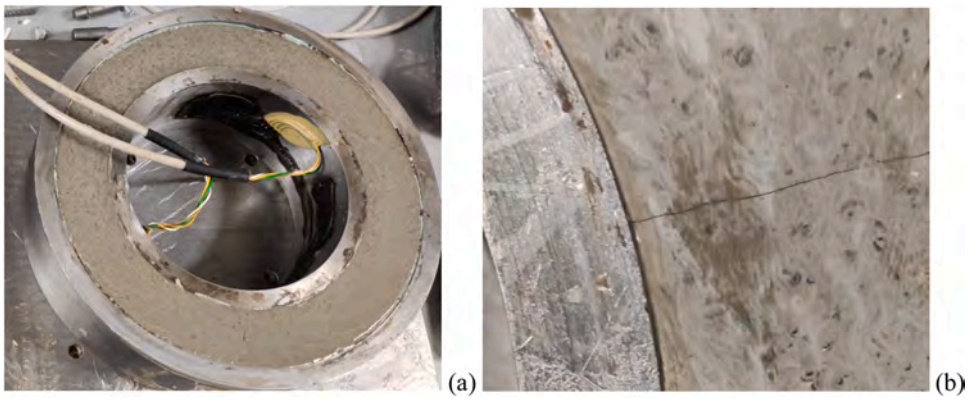

Fig. 27. Retrain ring test, a- before cracking, and b- after cracking.

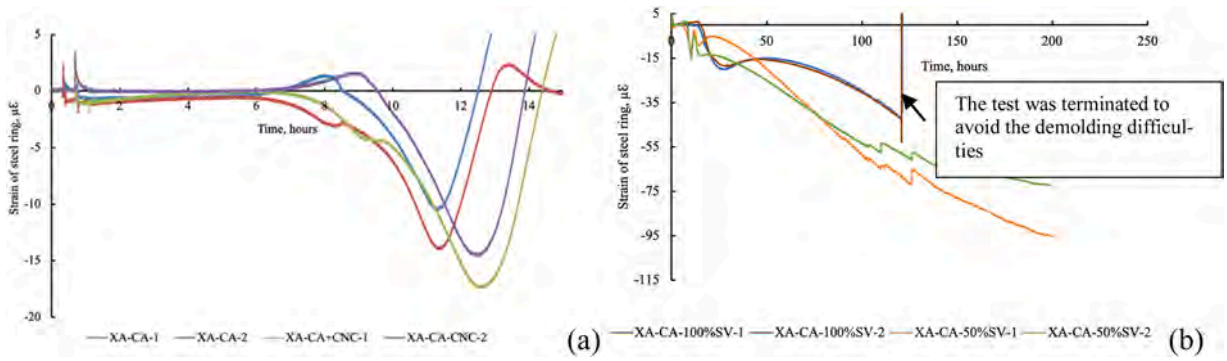

Fig. 28. Steel ring train versus age, a- for specimens without steel fiber, and b- for specimens with half and full amount of steel fiber content.

– Due to the UHPC high tensile elastic modulus, strength and ductility, reducing the wall thickness to 60 mm without any steel reinforcements or stiffening diaphragm did not affect the serviceability limit states in terms of deformability under service loads, the response of the structure remaining well within the elastic regime.
– Since the UHPC elements exhibited stress distribution capacity, most of strains measured at service water level reveals a strain level within the prescribed code limits, even though, the thickness of the wall has been tremendously reduced. For this reason, adopting

Fig. 29. Durability observations: geothermal water exposed surface condition from the second basin (left), and geothermal water exposed surface from the first basin (right).

thin UHPC section could result in revising the relationships between strain limits and structural slenderness (e.g. height to cross section depth ratio) prescribed in the Eurocode 2 part 3 for tightness purpose.
- Crack healing and sealing was clearly evident in the first and second compartments, where the shrinkage cracks have been effectively sealed after being subjected to moisture of geothermal water.
- To obtain the maximum efficiency of the UHPC, horizontal casting is preferred instead of casting UHPC vertically, to avoid steel fiber segregation and lack of homogenous distribution, unless limited height segmental casting is adopted.

Declaration of Competing Interest

The authors declare that they have no known competing financial interests or personal relationships that could have appeared to influence the work reported in this paper.

Acknowledgments

The activity described in this paper has been performed in the framework of the project “Rethinking coastal defense and Green-energy Service infrastructures through enHancEd-durAbiLity high-performance cement-based materials-ReSHEALience”, funded by the European Union Horizon 2020 research and innovation program under GA No. 760824. The information and views set out in this publication are those of the authors and do not necessarily reflect the official opinion of the European Commission.

The kind collaboration of Mr Antonio Cocco, Marco Cucchi, Daniele Spinelli and Marco Del Galdo, technicians at the Laboratory for Testing Materials Buildings and Structures (LPMSC), Politecnico di Milano in installation of strain gauges and in use-training for the equipment employed in the tests is gratefully acknowledged. The contribution is acknowledged also of Ph.D. students Davide di Summa, Antonio Cibelli, Niranjan Prabhu Kannikachalam, Bin Xi, Kasyapa Sriram Kompella, Giacomo Rizzieri and Andrea Marcucci and of M.Sc. thesis students Matteo Parpanesi, Giacomo Listrani, Simone Dicembre and Giovanni Recchia in performing the field measurement, in partial fulfillment of the requirements for the completion of the educational part of their programmes.

References

[1] S. Al-Obaidi, P. Bamonte, L. Ferrara, M. Luchini, I. Mazzantini, Durability-based design of structures made with ultra-high-performance/ultra-high-durability concrete in extremely aggressive scenarios: application to a geothermal water basin case study, Infrastructures 5 (2020) 1–44, https://doi.org/10.3390/infrastructures5110102.

[2] Davide di Summa, José Roberto Tenório Filho, Didier Snoeck, Philip Van den Heede, Sandra Van Vlierberghe, Liberato Ferrara, N.D. Belie, Environmental and economic sustainability of crack mitigation in reinforced concrete with super absorbent polymers (SAPs), J. Clean. Prod. (2022) (submitted).

[3] R. Folić, D. Zenunović, Durability problem of RC structures in Tuzla industrial zone — two case studies, Eng. Struct. 32 (2010) 1846–1860, https://doi.org/10.1016/J.ENGSTRUCT.2010.03.004.

[4] BSI Standards Publication Concrete-Specification, Performance, Production and Conformity, ISBN 9780580859663, 2014.

[5] Duy Quang Nguyen, Christopher Brammer, M. Bagajewicz, New tool for the evaluation of the scheduling of preventive maintenance for chemical process plants, Ind. Eng. Chem. Res. 47 (2008) 1910–1924, https://doi.org/10.1021/IE071231I.

[6] V. Marcos-Meson, M. Geiker, G. Fischer, A. Solgaard, U.H. Jakobsen, T. Danner, C. Edvardsen, T.L. Skovhus, A. Michel, Durability of cracked SFRC exposed to wet-dry cycles of chlorides and carbon dioxide – multiscale deterioration phenomena, Cem. Concr. Res. 135 (2020), 106120, https://doi.org/10.1016/J.CEMCONRES.2020.106120.

[7] T. Ishida, P.O.N. Iqbal, H.T.L. Anh, Modeling of chloride diffusivity coupled with non-linear binding capacity in sound and cracked concrete, Cem. Concr. Res. 39 (2009) 913–923, https://doi.org/10.1016/J.CEMCONRES.2009.07.014.

[8] Y. Ding, K.Q. Yu, J. Tao Yu, S. Xu lang, Structural behaviors of ultra-high performance engineered cementitious composites (UHP-ECC) beams subjected to bending-experimental study, Constr. Build. Mater. 177 (2018) 102–115, https://doi.org/10.1016/J.CONBUILDMAT.2018.05.122.

[9] E. Cuenca, L. D'Ambrosio, D. Lizunov, A. Tretjakov, O. Volobujeva, L. Ferrara, Mechanical properties and self-healing capacity of ultra high performance fibre reinforced concrete with alumina nano-fibres: tailoring ultra high durability concrete for aggressive exposure scenarios, Cem. Concr. Compos. 118 (2021), 103956, https://doi.org/10.1016/J.CEMCONCOMP.2021.103956.

[10] L. Ferrara, N. Ozyurt, M. Di Prisco, High mechanical performance of fibre reinforced cementitious composites: the role of "casting-flow induced" fibre orientation, Mater. Struct. Constr. 44 (2011) 109–128, https://doi.org/10.1617/s11527-010-9613-9.

[11] L. Ferrara, M. Cremonesi, M. Faifer, S. Toscani, L. Sorelli, M.A. Baril, J. Réthoré, F. Baby, F. Toutlemonde, S. Bernardi, Structural elements made with highly flowable UHPFRC: correlating computational fluid dynamics (CFD) predictions and non-destructive survey of fiber dispersion with failure modes, Eng. Struct. 133 (2017) 151–171, https://doi.org/10.1016/j.engstruct.2016.12.026.

[12] K. Yu, L. Li, J. Yu, Y. Wang, J. Ye, Q.F. Xu, Direct tensile properties of engineered cementitious composites: a review, Constr. Build. Mater. 165 (2018) 346–362, https://doi.org/10.1016/J.CONBUILDMAT.2017.12.124.

[13] K. Yu, L. Li, J. Yu, J. Xiao, J. Ye, Y. Wang, Feasibility of using ultra-high ductility cementitious composites for concrete structures without steel rebar, Eng. Struct. 170 (2018) 11–20, https://doi.org/10.1016/J.ENGSTRUCT.2018.05.037.

[14] M.C. Caruso, C. Pascale, E. Camacho, L. Ferrara, Comparative environmental and social life cycle assessments of off-shore aquaculture rafts made in ultra-high performance concrete (UHPC), Int. J. Life Cycle Assess. (1) (2022) 1–20, https://doi.org/10.1007/S11367-021-02017-6.

[15] K. Niranjan Prabhu, Davide di Summa, Ruben P. Borg, Estefania Cuenca, Matteo Parpanesi, Nele De Belie, L. Ferrara, Assessment of sustainability and self-fealing performances of recycled ultra-high performance concrete (R-UHPC), Acids Mater. J. (2022) (Submitted).

[16] F.P. Bos, C. Menna, M. Pradena, E. Kreiger, W.R.L. da Silva, A.U. Rehman, D. Weger, R.J.M. Wolfs, Y. Zhang, L. Ferrara, et al., The realities of additively manufactured concrete structures in practice, Cem. Concr. Res. 156 (2022), 106746, https://doi.org/10.1016/J.CEMCONRES.2022.106746.

[17] V. Mechtcherine, F.P. Bos, A. Perrot, W.R.L. da Silva, V.N. Nerella, S. Fataei, R.J.M. Wolfs, M. Sonebi, N. Roussel, Extrusion-based additive manufacturing with cement-based materials – production steps, processes, and their underlying physics: a review, Cem. Concr. Res. 132 (2020), 106037, https://doi.org/10.1016/J.CEMCONRES.2020.106037.

[18] E. Kreiger, B. Diggs-McGee, T. Wood, B. MacAllister, M. Kreiger, Field considerations for deploying additive construction. RILEM Bookseries 2020, 2020, pp. 1147–1163, https://doi.org/10.1007/978-3-030-49916-7_109.

[19] C. Menna, J. Mata-Falcón, F.P. Bos, G. Vantyghem, L. Ferrara, D. Asprone, T. Salet, W. Kaufmann, Opportunities and challenges for structural engineering of digitally fabricated concrete, Cem. Concr. Res. 133 (2020), 106079, https://doi.org/10.1016/J.CEMCONRES.2020.106079.

[20] R.A. Buswell, F.P. Bos, W.R.L. da Silva, N. Hack, H. Kloft, D. Lowke, N. Freund, A. Fromm, E. Dini, T. Wangler, et al., Digital fabrication with cement-based materials: process classification and case studies, RILEM State Art Rep. 36 (2022) 11–48, https://doi.org/10.1007/978-3-030-90535-4_2.

[21] K. Li, Durability design of concrete structures: phenomena, modelling and practice, Durab. Des. Concr. Struct. Phenom. Model. Pract. (2016) 1–280, https://doi.org/10.1002/9781118910108.

[23] F. Lo Monte, L. Ferrara, Tensile behaviour identification in ultra-high performance fibre reinforced cementitious composites: indirect tension tests and back analysis of flexural test results, Mater. Struct. Constr. 53 (2020) 1–12, https://doi.org/10.1617/s11527-020-01576-8.

[24] E. Cuenca, L. D'Ambrosio, D. Lizunov, A. Tretjakov, O. Volobujeva, L. Ferrara, Mechanical properties and self-healing capacity of ultra high performance fibre reinforced concrete with alumina nano-fibres: tailoring ultra high durability concrete for aggressive exposure scenarios, Cem. Concr. Compos. 118 (2021), 103956, https://doi.org/10.1016/j.cemconcomp.2021.103956.

[25] E. Cuenca, A. Mezzena, L. Ferrara, Synergy between crystalline admixtures and nano-constituents in enhancing autogenous healing capacity of cementitious composites under cracking and healing cycles in aggressive waters, Constr. Build. Mater. 266 (2021), 121447, https://doi.org/10.1016/j.conbuildmat.2020.121447.

[26] A. Cibelli, M. Pathirage, G. Cusatis, L. Ferrara, G. Di Luzio, A discrete numerical model for the effects of crack healing on the behaviour of ordinary plain concrete: Implementation, calibration, and validation, Eng. Fract. Mech. 263 (2022), 108266, https://doi.org/10.1016/J.ENGFRACMECH.2022.108266.

[27] E.J. Mezquida-Alcaraz, J. Navarro-Gregori, P. Serna-Ros, Direct procedure to characterize the tensile constitutive behavior of strain-softening and strain-hardening UHPFRC, Cem. Concr. Compos. 115 (2021), 103854, https://doi.org/10.1016/J.CEMCONCOMP.2020.103854.

[28] M. Giménez, M.C. Alonso, E. Menéndez, M. Criado, Durability of UHPFRC functionalised with nanoadditives due to synergies in the action of sulphate and chloride in cracked and uncracked states, Mater. Constr. 71 (2021), https://doi.org/10.3989/MC.2021.14021 e264–e264.

[29] M. Roig-Flores, R.P. Borg, C. Ruiz-Muñoz, E.J. Mezquida-Alcaraz, E. Giménez-Carbó, A.M. Lozano Násner, P. Serna, Preliminary study on the fresh and mechanical properties of UHPC made with recycled UHPC aggregates, Eur. J. Environ. Civ. Eng. (2021), https://doi.org/10.1080/19648189.2021.1997826.

[30] H. Doostkami, M. Roig-Flores, P. Serna, Self-healing efficiency of ultra high-performance fiber-reinforced concrete through permeability to chlorides, Constr. Build. Mater. 310 (2021), 125168, https://doi.org/10.1016/J.CONBUILDMAT.2021.125168.

[31] E.J. Mezquida-Alcaraz, J. Navarro-Gregori, J.R. Martí-Vargas, P. Serna-Ros, Effects of tension stiffening and shrinkage on the flexural behavior of reinforced UHPFRC beams, Case Stud. Constr. Mater. 15 (2021), e00746, https://doi.org/10.1016/J.CSCM.2021.E00746.

[32] E. Cuenca, F. Lo Monte, M. Moro, A. Schiona, L. Ferrara, Effects of autogenous and stimulated self-healing on durability and mechanical performance of UHPFRC: validation of tailored test method through multi-performance healing-induced recovery indices, Sustainability 13 (2021) 11386, https://doi.org/10.3390/SU132011386.

[33] Estefania Cuenca, Maria Criado, Mercedes Gimenz, Maria Cruz Alonso, L. Ferrara, Effects of alumina nanofibers and cellulose nanocrystals on durability and self-healing capacity of ultrahigh-performance fiber-reinforced concretes, ASCE J. Mater. Civ. Eng. (2022), https://doi.org/10.1061/(ASCE)MT.1943-5533.0004375.

[34] S. Al Obaidi, P. Bamonte, F. Animato, F. Lo Monte, I. Mazzantini, M. Luchini, S. Scalari, L. Ferrara, Innovative design concept of cooling water tanks/basins in geothermal power plants using ultra-high-performance fiber-reinforced concrete with enhanced durability, Sustainability 13 (2021) 9826, https://doi.org/10.3390/SU13179826.

[35] N. Europeenne, E. Norm, E. Version, European Standard Eurocode 2-Design of Concrete Structures-Part 3: Liquid Retaining and Containment Structures, Vol. 4, 1992.

[36] Al-Obaidi, Salam De Sandre, Fabio, L. Ferrara, Durability analysis of ultra high-performance fiber reinforced concrete structures in cracked serviceability limit state, in: Proceedings of the International Conference and Advances in Sustainable Construction Materials and Structures, Merida, Mexico, 2022 (In press).

[37] L. Ferrara, M. Faifer, S. Toscani, A magnetic method for non destructive monitoring of fiber dispersion and orientation in steel fiber reinforced cementitious composites-part 1: method calibration, Mater. Struct. Constr. 45 (2012) 575–589, https://doi.org/10.1617/s11527-011-9793-y.

[38] L. Ferrara, M. Faifer, M. Muhaxheri, S. Toscani, A magnetic method for non destructive monitoring of fiber dispersion and orientation in steel fiber reinforced cementitious composites. Part 2: correlation to tensile fracture toughness, Mater. Struct. Constr. 45 (2012) 591–598, https://doi.org/10.1617/s11527-011-9794-x.
[39] S. Gupta, S. Al-Obaidi, L. Ferrara, Meta-analysis and machine learning models to optimize the efficiency of self-healing capacity of cementitious material, Materials 14 (2021) 4437, https://doi.org/10.3390/MA14164437.
[40] S. Gupta, S. Al-Obaidi, L. Ferraral, State of the art on self-healing capacity of cementitious materials based on data mining strategies, Spec. Publ. 350 (2021) 27–44.